

1

2

3

4

5

6

7 **A single N6-methyladenosine site in lncRNA HOTAIR regulates its function
8 in breast cancer cells**

9

10 Authors: Allison M. Porman¹, Justin T. Roberts^{1,2}, Emily D. Duncan^{2,3}, Madeline L. Chrupcala^{1,4}, Ariel A.
11 Levine^{1,4}, Michelle A. Kennedy¹, Michelle M. Williams⁵, Jennifer K. Richer⁵, Aaron M. Johnson^{1,2,4,*}

12 Affiliations: ¹University of Colorado Anschutz Medical Campus, Biochemistry and Molecular Genetics
13 Department; ²University of Colorado Anschutz Medical Campus, Molecular Biology Graduate Program, ⁴
14 University of Colorado Anschutz Medical Campus, Cell and Developmental Biology; ⁴University of
15 Colorado Anschutz Medical Campus, RNA Bioscience Initiative ⁵Department of Pathology, University of
16 Colorado Anschutz Medical Campus Aurora, Colorado.

17

18 *Corresponding Author

19 Aaron M. Johnson, PhD

20 e-mail: Aaron.m.johnson@CUAnschutz.edu

21 Tel: +1(303)724-3224

22

23 **Abstract**

24 N6-methyladenosine (m6A) modification of RNA plays important roles in normal and cancer
25 biology, but knowledge of its function on long noncoding RNAs (lncRNAs) remains limited. Here, we
26 investigate whether m6A regulates the function of the human HOTAIR lncRNA, which contributes to
27 multiple pro-tumor phenotypes in triple-negative breast cancer (TNBC) cells. We identify at least 8
28 individual m6A sites within HOTAIR, with a single site (A783) consistently methylated. Mutation of A783
29 impairs cellular proliferation and invasion in HOTAIR-overexpressing TNBC cells. m6A at A783 regulates
30 HOTAIR's ability to localize to chromatin and induce gene pathways that affect tumor progression. In
31 contrast, A783U mutant HOTAIR demonstrates loss-of-function and antimorph behaviors by impairing
32 gene expression changes induced by WT HOTAIR and, in some cases, inducing opposite changes in
33 gene expression. HOTAIR interacts with nuclear m6A reader YTHDC1 and high HOTAIR is significantly
34 associated with shorter overall patient survival, particularly in the context of high *YTHDC1*. At the
35 molecular level, YTHDC1-HOTAIR interactions are required for chromatin localization and regulation of
36 gene repression. Our work demonstrates how modification of one base in a lncRNA can elicit a distinct
37 gene regulation mechanism and drive disease-associated phenotypic changes such as proliferation and
38 invasion.

39

40 **Introduction**

41 Long non-coding RNAs (lncRNAs) are becoming increasingly noted for their roles in
42 transcriptional regulation (Long, Wang, Youmans, & Cech, 2017). Members of this class of noncoding
43 RNAs are typically longer than 200 nucleotides, transcribed by RNA polymerase II, and processed
44 similarly to mRNAs (Esteller, 2011). lncRNAs regulate transcription in a variety of ways; they can alter
45 chromatin by directing histone-modifying enzymes to their target loci to induce changes in chromatin, or
46 can regulate transcription directly by interacting with transcription factors and RNA polymerase II (Long
47 et al., 2017). Importantly, lncRNAs are often key regulators of epigenetic changes that can drive cancer
48 progression, often by aberrant overexpression (Schmitt & Chang, 2016).

49 The human lncRNA HOTAIR is a 2.2kb spliced and polyadenylated RNA transcribed from the
50 HoxC locus. Originally identified as a developmental regulator acting in *trans* to repress expression of
51 the HoxD locus (Rinn et al., 2007), aberrant high levels of HOTAIR are associated with poor survival and
52 increased cancer metastasis in many different cancer types, including breast cancer (Balas & Johnson,
53 2018; Gupta et al., 2010). Exogenous overexpression of HOTAIR in the MDA-MB-231 TNBC cell line
54 results in the repression of hundreds of genes (Gupta et al., 2010), and it promotes cell invasion,
55 migration, proliferation, and self-renewal capacity in multiple breast cancer cell lines (Deng et al., 2017;
56 Gupta et al., 2010; Meredith, Balas, Sindy, Haislop, & Johnson, 2016). HOTAIR function is particularly
57 striking in MDA-MB-231 cells, given that this is already a highly invasive breast cancer cell line and its
58 invasiveness is increased even further by HOTAIR overexpression (Gupta et al., 2010; Meredith et al.,
59 2016). This is reflective of the prognostic impact of HOTAIR expression in TNBC patients where high
60 HOTAIR expression correlates with poorer overall survival (Gupta et al., 2010; Yang et al., 2011). MDA-
61 MB-231 cells express low levels of endogenous HOTAIR, offering an opportunity to study response to
62 HOTAIR transgenic overexpression, which is proposed to mimic the high levels of HOTAIR observed in
63 patients with aggressive TNBC (Gupta et al., 2010).

64 At its target loci, HOTAIR mediates the induction of H3K27 trimethylation (H3K27me3) by
65 Polycomb Repressive Complex 2 (PRC2), resulting in heterochromatin formation and repression (Gupta

66 et al., 2010; Tsai et al., 2010; Yansheng Wu et al., 2015). In cancer contexts, high levels of HOTAIR
67 misdirect this mechanism to loci that are not typically repressed in the tissue of origin(Balas & Johnson,
68 2018; Gupta et al., 2010; Hajjari & Salavaty, 2015). Despite these previous findings, a recent study
69 demonstrated that HOTAIR can repress genes even in the absence of PRC2, suggesting that initial
70 repression or transcriptional interference may occur upstream of H3K27me3 by PRC2(Portoso et al.,
71 2017) (Figure 1A).

72 HOTAIR also interacts with lysine-specific demethylase 1 (LSD1), a histone demethylase that
73 acts on H3K4me2, which has been proposed to reinforce repression by HOTAIR(L. Li et al., 2013;
74 Somarowthu et al., 2015; Tsai et al., 2010). A new study in human epithelial kidney cells found that
75 HOTAIR utilizes its LSD1-interacting domain to perturb LSD1 genomic distribution, independent of major
76 changes in H3K4me2, leading to increased invasion(Jarroux et al., 2021). In this context, HOTAIR is
77 proposed to inhibit the normal function of LSD1 in maintaining epithelial cells(Jarroux et al., 2021;
78 McDonald, Wu, Timp, Doi, & Feinberg, 2011; Wang et al., 2009). In light of these findings, how HOTAIR
79 specifically accomplishes transcriptional repression at its target loci, and how other pathways and cancer
80 contexts influence HOTAIR function, remain elusive.

81 N6-methyladenosine (m6A) is a reversible RNA modification. It has been well studied in
82 messenger RNAs (mRNAs), where it can regulate multiple steps of the mRNA life cycle, including
83 processing, decay, and translation(Shi, Wei, & He, 2019); however, how m6A regulates lncRNA-
84 mediated processes is less understood. Nevertheless, there is evidence for m6A regulation of lncRNAs.
85 For example, the lncRNA Xist, a key mediator of X chromosome inactivation, contains multiple m6A sites
86 that contribute to its ability to induce repression of the X chromosome(Coker et al., 2020; Patil et al.,
87 2016).

88 The m6A modification on an RNA is typically recognized by a “reader” protein that binds
89 specifically to methylated adenosine to mediate the functional outcome of m6A deposition. Apart from
90 the YTH family of proteins which contain the YTH domain that directly read m6A, a handful of non-
91 canonical indirect m6A readers have been suggested(Zaccara, Ries, & Jaffrey, 2019). In the case of Xist,

92 the canonical YTH-containing nuclear localized m6A reader YTHDC1 recognizes m6A on Xist to mediate
93 repression of the X chromosome(Nesterova et al., 2019; Patil et al., 2016). In contrast, m6A on *cis*-acting
94 chromatin-associated regulatory RNAs leads to their YTHDC1-dependent degradation, preventing
95 transcription of downstream genes(Jun Liu et al., 2020). Collectively, m6A influences the regulatory roles
96 of both mRNA and noncoding RNA via diverse mechanisms(Coker, Wei, & Brockdorff, 2019).

97 RNA modifications such as m6A have been shown to play critical roles in several human
98 cancers(X. Wu, Sang, & Gong, 2018). In breast cancer, studies have revealed that dysregulation of m6A
99 levels can generate breast cancer stem-like cells and promote metastasis(Niu et al., 2019; C. Zhang et
100 al., 2016; J. X. Zhang et al., 2013). Of the currently designated m6A reader proteins, we have previously
101 shown that hnRNP A2/B1, a proposed non-canonical reader lacking the m6A-binding YTH domain, can
102 interact with HOTAIR to regulate its chromatin and cancer biology mechanisms by promoting HOTAIR
103 interactions with target mRNAs(Meredith et al., 2016). This evidence suggests that m6A may play a role
104 in cancers where HOTAIR is overexpressed.

105 Here, we set out to investigate the potential function of m6A in HOTAIR-mediated breast cancer
106 growth and invasion. We identify at least 8 m6A sites in HOTAIR and show that a single site (A783) is
107 required for HOTAIR-mediated TNBC growth and invasion. Mutation of adenosine 783 in HOTAIR to
108 uracil prevents the normal chromatin association and gene expression changes that are induced by the
109 wild-type lncRNA. Surprisingly, the A783U mutant induces opposite gene expression changes to wild-
110 type HOTAIR, reducing cancer phenotypes in TNBC cells, suggesting that the mutant HOTAIR is an
111 antimorph. We find that YTHDC1, the nuclear m6A reader, interacts with HOTAIR at methylated A783
112 and artificial tethering of YTHDC1 at this site is sufficient to restore HOTAIR chromatin association in the
113 A783 mutant. Finally, using a reporter system, we show that YTHDC1 mediates repression by HOTAIR
114 in the absence of PRC2. Overall, our results suggest a model where a single site of m6A modification on
115 HOTAIR enables a strong interaction with YTHDC1 to retain HOTAIR on chromatin for repression of its
116 target genes, leading to altered TNBC properties. Collectively, our results demonstrate the potent activity
117 of m6A on lncRNAs and in turn their role in cancer.

118

119 **Results**

120 **HOTAIR contains multiple sites of m6A modification in breast cancer cell lines**

121 To investigate the possibility that m6A regulates the function of HOTAIR in a mechanism similar
122 to its regulation of lncRNA Xist, we examined previous genome-wide maps of m6A sites in human cells.
123 Using the CVm6A database(Han et al., 2019), we found 3 m6A peaks in HOTAIR in HeLa cells, although
124 the enrichment score for these sites was low(Figure 1 – figure supplement 1). To evaluate m6A
125 methylation of HOTAIR in relevant breast cancer cells, we performed m6A RNA immunoprecipitation
126 (meRIP) qRT-PCR in MCF-7 cells, which express low levels of endogenous HOTAIR(Meredith et al.,
127 2016). A significant portion of HOTAIR was recovered upon immunoprecipitation with the anti-m6A
128 antibody (26.2%, p=0.006), similar to an m6A modified region on the positive control region of *EEF1A1*,
129 and consistently higher than a distal region of *EEF1A1* that is not m6A modified (Figure 1B).

130 We further found that m6A modification of HOTAIR is maintained during ectopic expression of
131 HOTAIR in a stable MDA-MB-231 cell line. meRIP in MDA-MB-231 cells expressing transgenic HOTAIR
132 resulted in significant HOTAIR recovery (27.1%, p=0.0009) (Figure 1C). These results demonstrate that
133 HOTAIR is m6A modified in two distinct breast cancer contexts.

134 To identify single nucleotide sites of m6A modification, we performed a modified m6A eCLIP
135 protocol(Roberts, Porman, & Johnson, 2020) on polyA-selected RNA from MCF-7 and MDA-MB-231
136 breast cancer cells (Figure 1 – figure supplement 2). In MCF-7 cells, we identified one m6A site within
137 the HOTAIR transcript at adenosine 783 (Figure 1D, Table S1). m6A at adenosine 783 in MDA-MB-231
138 cells with transgenic HOTAIR was consistently detected with high confidence (Table S1), along with 7
139 other sites using our multi-replicate consensus approach (Roberts et al., 2020) (Table S2). Of note, A783
140 occurred within a non-canonical ‘GAACG’ sequence located in an unstructured region of the HOTAIR
141 secondary structure(Somarowthu et al., 2015) (Figure 1 – figure supplement 3A).

142 To test if HOTAIR is m6A modified by the canonical m6A methyltransferase METTL3/14 complex,
143 we performed shRNA mediated depletion of METTL3, METTL14, and the adaptor protein WTAP in MCF-
144 7 cells (Figure 1 – figure supplement 4B). We observed a ~3 to 5-fold reduced recovery of HOTAIR in
145 methyltransferase-depleted cells relative to non-targeting controls ($p=0.0063$) (Figure 1 – figure
146 supplement 4C). Together, these results indicate that m6A methylation of HOTAIR is dependent on the
147 METTL3/14 complex.

148

149 **Nucleotide A783 is important for the ability of HOTAIR to promote breast cancer cell proliferation
150 and invasion**

151 Given that nucleotide A783 was consistently methylated within HOTAIR in our m6A mapping
152 experiments, in both endogenous and overexpressed contexts, we asked whether this modification had
153 any consequences to HOTAIR function. To directly test the functional role of A783, we mutated the
154 adenose to uracil at this position (HOTAIR^{A783U}). We then mapped m6A sites in MDA-MB-231 cells
155 overexpressing the HOTAIR^{A783U} mutant as above (Table S1). Both wild-type (WT) and the mutant form
156 of HOTAIR were expressed at similar levels, with approximately 5,000 transcripts per cell (Figure 1E),
157 resembling the high levels of HOTAIR observed in samples from cancer patients (Arshi A, Raeisi F,
158 Mahmoudi E, Mohajerani F, Kabiri H, Fazel R, Zabihian-Langeroudi M, 2020; Gupta et al., 2010; Yang
159 et al., 2011). While the CLIP-based m6A signature was no longer detected at adenose 783 when this
160 site was mutated to uracil, we detected m6A modification at five of the seven other multi-replicate
161 consensus sites (Tables S1 and S2, Figure 1B). Nucleotides 143 and 620 were no longer called with
162 multi-replicate consensus confidence as m6A in the A783U mutant, though m6A143 was only called in
163 WT HOTAIR at our lowest confidence category and m6A620 is called in one of the A783U mutant
164 replicates (Table S1). Nonetheless, it is possible that methylation at A783 is required for one or both m6A
165 events to occur.

166 To determine the effect of the A783U mutation on HOTAIR-mediated breast cancer cell growth,
167 we measured the doubling time of MDA-MB-231 cells expressing WT and A783U mutant HOTAIR. As

168 described above, we overexpressed HOTAIR and the HOTAIR^{A783U} mutant in MDA-MB-231 cells and
169 included overexpression of an antisense sequence of luciferase mRNA (Anti-Luc) as a negative
170 control(Meredith et al., 2016). Similar to previous studies, transgenic overexpression of HOTAIR resulted
171 in 10³-10⁴ copies of HOTAIR per cell and mediated increased cancer growth and invasion of MDA-MB-
172 231 cells(Gupta et al., 2010) (Figure 1E-G). We performed cell proliferation assays by plating 5,000 cells
173 in a 96-well dish and analyzing confluence every 2 hours over a period of 48 hours (example shown in
174 Figure 1 – figure supplement 3B). We observed that MDA-MB-231 cells overexpressing WT HOTAIR
175 proliferated more quickly, with a shorter doubling time (~26 hours) than cells overexpressing Anti-Luc
176 (~28.5 hours, p=0.0003) (Figure 1F and Figure 1 – figure supplement 3C). Surprisingly, the single
177 nucleotide mutation of A783U in HOTAIR abolished its ability to enhance MDA-MB-231 cell proliferation;
178 cells expressing HOTAIR^{A783U} proliferated more slowly, with a longer doubling time than those expressing
179 WT HOTAIR (~28.6 hours, p=0.004) and grew similarly to cells containing the Anti-Luc control. To
180 examine the role of A783 of HOTAIR in mediating breast cancer cell invasion, the same MDA-MB-231
181 cell lines were plated in a Matrigel invasion assay. Overexpression of WT HOTAIR induced a significant
182 increase in number of cells invaded compared to the Anti-Luc control (p=0.038). In contrast,
183 overexpression of A783U HOTAIR did not lead to an increase in invasion compared to the Anti-Luc
184 control (p=0.22) and resulted in significantly less cells invaded compared to overexpression of WT
185 HOTAIR (p=0.012) (Figure 1G). Altogether, these results suggest that m6A modification of adenosine
186 783 in HOTAIR is key for mediating the increased aggressiveness of TNBC that is promoted in contexts
187 where the lncRNA is overexpressed.

188

189 **Overexpression of A783U mutant HOTAIR induces divergent gene expression changes from wild-
190 type HOTAIR in breast cancer cells**

191 To analyze HOTAIR-mediated gene expression changes in MDA-MB-231 cells, we performed
192 high throughput RNA sequencing on cells overexpressing WT HOTAIR, A783U mutant HOTAIR, or
193 antisense luciferase as a control. For cells expressing WT HOTAIR, we identified 155 genes that were

194 differentially expressed (adjusted $p<0.1$) when compared with control cells expressing Anti-Luciferase
195 (Figure 2A). Upregulated genes in cells expressing WT HOTAIR include genes involved in positive
196 regulation of angiogenesis ($p=1.22E-05$), regulation of cell population proliferation ($p=0.0361$), and cell
197 differentiation ($p=0.0157$), while downregulated genes include genes involved in cell adhesion
198 ($p=0.0118$), p53 ($p=0.0112$) and MAPK ($p=0.0313$) signaling, and tumor repressors such as HIC1 and
199 DMNT3A. This set of genes had significantly different expression in cells overexpressing WT HOTAIR
200 compared to either cells overexpressing Anti-Luciferase or the A783U mutant HOTAIR (Figure 2A-C).
201 Surprisingly, mutation of A783 did not merely prevent most gene expression changes seen in wild-type
202 HOTAIR, but instead, expression of the A783U mutant induced certain changes in the opposite direction
203 from the baseline control MDA-MB-231 cell line. We confirmed this pattern by qRT-PCR: genes that were
204 upregulated in MDA-MB-231 cells upon introduction of WT HOTAIR had decreased expression in cells
205 with A783U mutant HOTAIR (Figure 2B). This included genes such as *PTK7* involved in the Wnt signaling
206 pathway (fold change relative to control in WT HOTAIR=2.6, $p=0.008$; in A783U HOTAIR=-1.4, $p=0.002$);
207 *CDH11*, a mesenchymal cadherin that is upregulated in invasive breast cancer cell lines(Pishvaian et al.,
208 1999) (fold change in WT HOTAIR=2.0, $p=0.01$; in A783U HOTAIR=-1.6, $p=0.02$); and *GRIN2A*, an
209 oncogenic glutamate receptor (fold change in WT HOTAIR=2.5, $p=0.006$; in A783U HOTAIR=-3.7,
210 $p=9.3E-05$). Similarly, genes downregulated with WT HOTAIR were significantly increased with A783U
211 HOTAIR, compared to the parental MDA-MB-231 control, including *SEMA5A*, a guidance cue protein
212 that suppresses the proliferation and migration of lung adenocarcinoma cells(Ko et al., 2020) (fold change
213 relative to control in WT HOTAIR=-3.5, $p=0.0002$; in A783U HOTAIR=2.8, $p=0.01$); *SIRPA*, a cell surface
214 receptor that can act as a negative regulator of the phosphatidylinositol 3-kinase signaling and mitogen-
215 activated protein kinase pathways(Takahashi, 2018) (fold change in WT HOTAIR=-1.6, $p=0.03$; in A783U
216 HOTAIR=3.1, $p=0.009$); and *TP53I11*, a p53-interacting protein that suppresses migration and
217 metastasis in MDA-MB-231 cells(Xiao et al., 2019) (fold change in WT HOTAIR=-1.7, $p=0.03$; in A783U
218 HOTAIR=4.0, $p=0.008$) (Figure 2C). To further analyze differences in cells expressing A783U mutant
219 HOTAIR, we performed a pairwise comparison with control MDA-MB-231 cells and identified 758
220 differentially expressed genes (Figure 2D). Upregulated gene categories in A783U HOTAIR-expressing

221 cells include negative regulation of response to growth factor stimulus ($p=2.27E-04$), positive regulation
222 of apoptosis ($p=3.88E-04$), and regulation of migration ($p=4.36E-04$), while downregulated gene
223 categories include regulation of the epithelial to mesenchymal transition ($p=1.48E-04$), angiogenesis
224 ($p=1.64E-04$), cell adhesion ($p=7.51E-05$), and cell migration ($p=1.64E-04$). We hypothesize that this
225 altered pattern of gene expression may underlie the slight decrease in cell invasion observed in the
226 A783U context compared to control MDA-MB-231 cells (Figure 1G).

227 To further investigate differences between cells expressing WT HOTAIR versus the A783U
228 mutant HOTAIR, we performed a pairwise comparison. Here, we observed the most differentially
229 expressed genes (2060) compared to other pairwise comparisons (Figure 2E, top). Overall, these results
230 reveal that expression of the A783U mutant HOTAIR induces additional and often opposite gene
231 expression changes compared to expression of WT HOTAIR in breast cancer cells, suggesting a
232 potential antimorph property of this single nucleotide mutation. The opposite gene expression pattern is
233 evident in the heat map of all differentially expressed genes (Figure 2 – Figure Supplement 1A), as well
234 as the observation that most (137/155, 88%) of WT HOTAIR-regulated genes have altered expression
235 with A783U HOTAIR, with a significant portion (46/155, 30%) having opposite expression in MDA-MB-
236 231 cells expressing A783U HOTAIR compared to control cells (Figure 2E, Figure 2 – Figure Supplement
237 1B-C). This pattern is also evident in the negative correlation (-0.48) when fold change in expression for
238 HOTAIR v Control and A783U v Control is plotted (Figure 2E, bottom). We hypothesized that prevention
239 of m6A methylation by the A783U mutation disrupts an m6A-dependent function to cause loss-of-function
240 and antimorph cell biology and gene expression behaviors.

241

242 **hnRNP B1 is not a direct m6A reader in MCF-7 cells**

243 We next sought to address the mechanisms behind HOTAIR m6A783 function. hnRNP A2/B1
244 has previously been suggested to be a reader of m6A, and the B1 isoform has a high affinity for binding
245 HOTAIR(Alarcon et al., 2015; Meredith et al., 2016; Yingmin Wu et al., 2019). However, comparing our
246 previously generated eCLIP results for hnRNP B1(Nguyen, Balas, Griffin, Roberts, & Johnson, 2018) to

247 the m6A eCLIP, both performed in MCF-7 cells, we found that, out of 10,470 m6A sites, only 417 (4%)
248 were identified to contain an hnRNP B1 binding site within 1,000 nucleotides (Figure 3 – figure
249 supplement 1A). Upon mapping hnRNP B1 signal intensity relative to the nearby m6A site, we observed
250 that hnRNP B1 is depleted directly over m6A sites (Figure 3 – figure supplement 1B). These results
251 suggest that hnRNP B1 is not a direct m6A reader, although m6A may indirectly promote its recruitment
252 in some contexts. When comparing hnRNP B1 binding in HOTAIR with m6A sites, B1 binding peaks in
253 MCF-7 cells occur in m6A-free regions of HOTAIR. Conversely, data from *in vitro* eCLIP analysis of B1
254 binding to unmodified HOTAIR reveal additional B1 binding peaks in Domain 1 of HOTAIR, one of which
255 occurs near several m6A sites (Figure 3 – figure supplement 1C). Altogether, these data suggest that
256 m6A is not likely to directly recruit hnRNP B1 as a reader, although it could contribute to hnRNP B1
257 binding.

258

259 **YTHDC1 interacts with HOTAIR to mediate breast cancer proliferation**

260 In light of the results for hnRNP A2B1 described above, we turned to alternative candidate m6A
261 readers of HOTAIR. YTHDC1 is a nuclear-localized m6A reader that binds m6A sites in noncoding RNAs,
262 including the Xist lncRNA (Patil et al., 2016). We reasoned that YTHDC1 was a strong candidate for
263 interaction with HOTAIR, which is a lncRNA that is also primarily nuclear-localized. To determine if
264 YTHDC1 interacts with HOTAIR, we performed RNA immunoprecipitation (RIP) qRT-PCR using an
265 antibody to YTHDC1. In both MDA-MB-231 cells overexpressing transgenic HOTAIR, and MCF-7 cells
266 expressing endogenous HOTAIR, a significant portion of HOTAIR RNA was recovered when using
267 antibodies specific against YTHDC1 (17.4%, p=0.04; 2.6%, p=0.003, respectively) (Figure 3A-B).

268 To test the role of YTHDC1 in HOTAIR's ability to enhance breast cancer cell proliferation, we
269 stably overexpressed or knocked down YTHDC1 in the context of WT or A783U HOTAIR overexpression
270 in MDA-MB-231 cells (Figure 3C-D). We noted that YTHDC1 protein levels tended to be ~2-fold higher
271 in cells containing WT HOTAIR compared to A783U mutant HOTAIR (Figure 3D). Although this difference
272 was not significant (p=0.16), it suggests a potential positive relationship between WT HOTAIR RNA and

273 YTHDC1 protein levels. Next, we used the MDA-MB-231 cell lines we generated to analyze proliferation
274 as described above. Growth of MDA-MB-231 cells overexpressing WT HOTAIR was not significantly
275 altered by YTHDC1 dosage (0.96 fold change, $p=0.16$ for pLX-DC1; 1.08 fold change, $p=0.26$ for shDC1,
276 respectively), yet there was a trend towards decreased doubling time with increasing YTHDC1. In
277 contrast, cells with A783U mutant HOTAIR had significant differences in doubling time with
278 overexpression or knockdown of YTHDC1 (Figure 3E). Overexpression of YTHDC1 led to significantly
279 faster growth of MDA-MB-231 cells containing A783U mutant HOTAIR (0.84-fold change in doubling
280 time, $p=0.003$), with proliferation rates comparable to cells expressing WT HOTAIR. Knockdown of
281 YTHDC1 in cells containing HOTAIR^{A783U} was particularly potent in reducing the growth rate (~1.2-fold
282 increase in doubling time, $p=0.008$) demonstrating a role for YTHDC1 in mediating HOTAIR's ability to
283 enhance proliferation of breast cancer cells through A783, or via other m6A sites in A783U mutant
284 HOTAIR upon YTHDC1 overexpression.

285

286 **High HOTAIR levels are associated with an aggressive disease progression in breast cancer
287 patients with high tumor YTHDC1 expression**

288 To further explore a clinical role for HOTAIR and YTHDC1 in breast cancer, we used GEPIA2, a
289 web server for large-scale expression profiling and interactive analysis (Tang, Kang, Li, Chen, & Zhang,
290 2019). To this end, we analyzed the relationship of *HOTAIR* and *YTHDC1* expression in publicly available
291 outcomes data from breast cancer patient primary tumors. Across all breast cancer patient samples,
292 *YTHDC1* is generally expressed at the mRNA level, ranging roughly five-fold. HOTAIR levels vary more
293 widely, with some samples not expressing the lncRNA. Because of these different expression profiles,
294 there is only a very modest positive correlation between *HOTAIR* and *YTHDC1* ($R=0.092$, $p=0.0025$)
295 (Figure 4 – figure supplement 1A). To further investigate *HOTAIR* and *YTHDC1* in breast tumors, we
296 used the Kaplan-Meier Plotter to analyze recurrence-free and overall survival of breast cancer
297 patients (Gyorffy et al., 2010) as well as UALCAN (a tool for analyzing cancer OMICS data) to determine
298 gene expression in normal breast tissue versus breast tumor specimens (Chandrashekhar et al., 2017).

299 Consistent with previous studies, high expression of *HOTAIR* is indicative of a shorter time to recurrence
300 (HR=1.41, p=6.3e-05) (Figure 4A) and shorter overall survival (HR=1.65, p=0.0084) (Figure 4 – figure
301 supplement 1B)(Arshi A, Raeisi F, Mahmoudi E, Mohajerani F, Kabiri H, Fazel R, Zabihian-Langeroudi
302 M, 2020; Gupta et al., 2010). *HOTAIR* RNA expression is increased in breast cancer specimens ~7-fold
303 compared to normal breast tissues (p=1.62e-12), with the highest *HOTAIR* expression (~14.5-fold
304 increase) observed in Stage 4 disease (p=5.36e-04) (Figure 4 – figure supplement 1C-D). The reverse
305 is true for *YTHDC1*, with high levels corresponding to longer disease-free status (HR=0.69, p=2.5e-11)
306 (Figure 4B) and overall survival (HR=0.73, p=0.0088) (Figure 4 – figure supplement 2A) and a modest
307 decrease (~10%) in mRNA levels in tumor compared to normal tissue (p=1.14e-06) (Figure 4C, Figure 4
308 – figure supplement 2B). Interestingly, *YTHDC1* protein is higher in tumor samples compared to normal
309 tissue (p=6.7e-09) (Figure 4D, Figure 4 – figure supplement 2C). This could be because in general there
310 are fewer epithelial cells in normal breast compared to the number of carcinoma cells in breast
311 tumors(Rezaul et al., 2010), and may suggest a significant amount of translational regulation for the
312 *YTHDC1* mRNA.

313 To examine *YTHDC1* in relation to *HOTAIR* in breast cancer outcomes, we assessed recurrence-
314 free and overall survival based on *HOTAIR* expression in cohorts of tumors expressing either high or low
315 levels of *YTHDC1* mRNA. In the context of high *YTHDC1* expression, *HOTAIR* is even more strongly
316 indicative of risk for shorter time to recurrence (HR=1.93, p=3.2e-05) (Figure 4E) and shorter overall
317 survival (HR=2.1, p=0.0012) (Figure 4 – figure supplement 2D) compared to *HOTAIR* alone (Figures 4B,
318 S6B). On the background of low *YTHDC1*, *HOTAIR* has a less impressive effect on disease-free survival
319 (HR=1.33, p=0.007) (Figure 4F), more similar to the effect of *HOTAIR* alone (Figure 4B), and on overall
320 survival, where *HOTAIR* expression is no longer a significant prognostic indicator (HR=1.34, p=0.23)
321 (Figure 4 – figure supplement 2E). Altogether, these patient outcomes data are consistent with high
322 *YTHDC1* levels potentially contributing to the ability of *HOTAIR* to affect breast cancer progression.

323

324 **Mutation at A783 of HOTAIR results in decreased interaction with YTHDC1 *in vitro*, but does not**
325 **abolish HOTAIR methylation or YTHDC1 interaction at other sites *in vivo***

326 To determine if nucleotide A783 in HOTAIR recruits YTHDC1 via m6A modification, we generated
327 PP7-tagged *in vitro* transcribed RNA of domain 2 of WT or A783U mutant HOTAIR and performed *in vitro*
328 m6A methylation with purified METTL3/14(Jianzhao Liu et al., 2014) and S-adenosylmethionine as a
329 methyl donor. We then transfected HEK293 cells with an expression plasmid containing FLAG-tagged
330 YTHDC1 and obtained protein lysates. The *in vitro* HOTAIR transcripts were tethered to IgG-coupled
331 magnetic beads via a PP7-Protein A fusion protein and incubated with FLAG-YTHDC1-containing protein
332 lysates. Beads were washed and the relative recovery of FLAG-YTHDC1 was determined by anti-FLAG
333 Western Blot (Figure 5A). WT HOTAIR interaction with YTHDC1 was enhanced when the transcript was
334 m6A-modified (~3-fold increase, p=0.04), while A783U HOTAIR interaction with YTHDC1 was not
335 significantly altered by the addition of m6A (~1.3-fold change, p=0.6) (Figure 5B-C).

336 To characterize changes to the molecular interactions that occur with mutation of A783 in breast
337 cancer cells, we performed m6A and YTHDC1 RIP experiments on MDA-MB-231 cells overexpressing
338 WT or A783U HOTAIR (Figure 5 – figure supplement 1A-B). Surprisingly, we did not see any significant
339 changes in HOTAIR recovery in either experiment (~1.2-fold change, p=0.5; 1.1-fold change, p=0.8 for
340 m6A and YTHDC1 RIP, respectively). The HOTAIR^{A783U} maintains m6A modifications at other sites within
341 the RNA, which we have mapped in the overexpression context (Table S1). These sites are likely
342 sufficient for HOTAIR recovery when immunoprecipitating YTHDC1. However, modification of A783, in
343 particular, appears to be important in mediating the physiological effects observed by HOTAIR
344 overexpression, likely by YTHDC1 binding to A783 in a methylation-dependent manner, as observed in
345 the *in vitro* experiment (Figure 5B-C).

346

347 **m6A and YTHDC1 mediate chromatin association and expression of HOTAIR**

348 Based on the differences observed between cell lines containing WT and A783U HOTAIR and
349 the function of HOTAIR in chromatin-mediated gene repression, we investigated whether chromatin
350 association of HOTAIR was altered in these cells. We performed fractionation of MDA-MB-231 cells
351 containing WT or A783U HOTAIR or an antisense-Luciferase control into cytoplasm, nucleoplasm, and
352 chromatin fractions (Figure 5D, see Methods). We isolated RNA from each fraction and performed qRT-
353 PCR for HOTAIR and GAPDH. Cells overexpressing WT HOTAIR had significantly more chromatin-
354 associated HOTAIR (~4.3-fold) than cells expressing A783U HOTAIR ($p<0.05$) (Figure 5E), though
355 overall levels of HOTAIR are unchanged (Figure 2A).

356 To examine the effect of YTHDC1 levels on HOTAIR chromatin association, we performed a
357 similar fractionation experiment in MDA-MB-231 cells expressing WT or A783U HOTAIR with
358 overexpression or knockdown of YTHDC1 (Figure 5 – figure supplement 1C). While YTHDC1 levels did
359 not significantly alter WT HOTAIR chromatin association, overexpression of YTHDC1 increased
360 HOTAIR^{A783U} chromatin association ~1.9-fold to similar levels as WT HOTAIR ($p=0.05$), and knockdown
361 resulted in a significant ~10-fold decrease in chromatin association ($p=0.01$) (Figure 5F). We reason that
362 the differences observed between WT and A783U mutant HOTAIR are due to a high affinity constitutive
363 interaction of YTHDC1 with WT HOTAIR at m6A783 that enables chromatin association and is not
364 affected by knockdown or overexpression. For A783U mutant HOTAIR that does not interact with
365 YTHDC1 at this position, increasing the concentration of YTHDC1 can drive interaction at other (lower
366 affinity) m6A sites within the mutated HOTAIR. These interactions occur at a low level in cells with wild-
367 type YTHDC1 levels, and, since they are low affinity, are most sensitive to knockdown of YTHDC1 (Figure
368 5 – Figure Supplement 1D). Therefore, the A783U mutant, which only retains these proposed lower
369 affinity sites, is particularly sensitive to YTHDC1 levels.

370 While HOTAIR expression levels remained similar for DC1 overexpression lines compared to
371 shNT control lines (0.8 fold change, $p=0.3$), they were significantly decreased by ~5 to 10-fold in YTHDC1
372 knockdown lines for both WT and A783U mutant HOTAIR relative to shNT cell lines ($p=3.24e-10$) (Figure
373 5G). These results suggest that YTHDC1 regulates the expression or stability of HOTAIR, independently

374 of A783. To investigate the role of other m6A sites within HOTAIR, we generated HOTAIR overexpression
375 constructs containing 6 or 14 adenosine-to-uracil mutations (6xAU and 14xAU, respectively) both of
376 which included A783U. While WT and A783U HOTAIR expression levels were similarly high, there was
377 a ~50-fold decrease in expression of 6xAU or 14xAU HOTAIR (Figure 5H). This suggests that other m6A
378 sites within HOTAIR mediate its high expression levels in breast cancer cells.

379

380 **Tethering YTHDC1 to A783U mutant HOTAIR restores chromatin association**

381 To more directly examine the effects of YTHDC1 interaction with HOTAIR in the context of the
382 A783U mutation, we employed a catalytically inactive RNA-targeting Cas protein, dCasRX, which has
383 previously been used to recruit effectors to specific RNA molecules via a guide RNA (Figure
384 6A)(Konermann et al., 2018). We transfected MDA-MB-231 cells stably expressing WT or A783U
385 HOTAIR with a plasmid containing the dCasRX-YTHDC1 fusion protein, in combination with a plasmid
386 containing either a HOTAIR guide RNA (targeting a 22-nucleotide sequence 7 nucleotides downstream
387 from A783 in HOTAIR, see Figure 6A) or a non-targeting gRNA. Expression of dCasRX-YTHDC1 was
388 confirmed by Western blot (Figure 6B). While chromatin association of WT HOTAIR remained
389 consistently high, chromatin association levels of A783U HOTAIR were only restored to near WT HOTAIR
390 levels upon transfection with plasmids containing the dCasRX-YTHDC1 fusion protein and the HOTAIR
391 gRNA ($p=0.25$ compared to WT HOTAIR). In contrast, chromatin association of A783U HOTAIR
392 remained low upon transfection of dCasRX-YTHDC1 with a non-targeting guide RNA (~3.7 fold lower
393 than WT HOTAIR, $p=0.0066$) (Figure 6C). HOTAIR RNA levels remained consistent in all samples
394 (Figure 6D). These results confirm that YTHDC1 mediates chromatin localization of HOTAIR, and show
395 that the chromatin association defect of the A783U mutation can be restored simply by restoring binding
396 of YTHDC1 at that specific location.

397

398 **YTHDC1 contributes to gene repression by HOTAIR in the absence of PRC2, independent of its**
399 **role in chromatin association or RNA stability**

400 To determine the effect of YTHDC1 on transcriptional repression mediated by HOTAIR, we used
401 previously generated reporter cell lines that contain HOTAIR artificially directly tethered to chromatin
402 upstream of a luciferase reporter gene to repress expression, independent of PRC2(Portoso et al., 2017)
403 (Figure 7A). We confirmed that HOTAIR tethered upstream of the luciferase reporter reduced luciferase
404 expression using both qRT-PCR (~2.3-fold lower, $p=8.0e-12$) and luciferase assay (~3.1-fold lower,
405 $p=0.002$) (Figure 7B,C). We also performed m6A eCLIP to confirm that *HOTAIR* was m6A modified in
406 this context and detected 10 m6A sites within *HOTAIR*, including A783 (Table S1). To test the role of
407 YTHDC1 in the repression mediated by HOTAIR, we used 3 different siRNAs to knock down YTHDC1
408 relative to a non-targeting control (~2-fold decrease in protein levels, $p=0.02$) in the HOTAIR-tethered
409 cells lacking the essential PRC2 subunit EED (Figure 7D). Knockdown of YTHDC1 resulted in
410 significantly higher luciferase RNA levels in these cells (~2.1 fold change, $p=2.2e-05$) (Figure 7E).
411 Luciferase enzymatic activity also increased upon YTHDC1 knockdown (~1.3 fold change, $p=0.03$)
412 (Figure 7F). YTHDC1 knockdown did not affect *HOTAIR* RNA levels in this context (~1.2-fold increase,
413 $p=0.8$) (Figure 7 – figure supplement 1A-B), indicating that the effects observed on luciferase expression
414 were likely due to disruption of the HOTAIR gene repression mechanism via depletion of YTHDC1 protein
415 rather than loss of HOTAIR expression.

416

417 **Discussion**

418 Similar to m6A regulation of mRNAs, it is becoming evident that m6A on lncRNAs is both
419 functionally diverse and context dependent. Here, we demonstrate that m6A and the m6A reader
420 YTHDC1 function to enable transcriptional repression by HOTAIR which is analogous to one of the
421 repressive functions demonstrated for the lncRNA Xist(Nesterova et al., 2019; Patil et al., 2016). Our
422 results reveal a mechanism whereby m6A modification of HOTAIR at a specific adenine residue

423 mediates interaction with YTHDC1, in turn enabling transcriptional interference by HOTAIR which
424 enhances TNBC properties including proliferation and invasion.

425 Function of specific m6A sites in HOTAIR

426 While several m6A sites were identified within HOTAIR when overexpressed, we only detected
427 one m6A site in the endogenously expressed context in MCF-7 cells, making it the most consistently
428 present methylation site. MDA-MB-231 cells overexpressing HOTAIR containing a mutation of this single
429 m6A-modified adenosine had a defect in HOTAIR-mediated proliferation and invasion, as well as its
430 ability to induce HOTAIR-mediated gene expression changes. While A783U mutant HOTAIR appears to
431 retain m6A modification at other sites and interaction with YTHDC1 *in vivo*, we note that the *in vivo*
432 analysis employs formaldehyde crosslinking prior to immunoprecipitation with the YTHDC1 antibody,
433 which enables detection of both weak and strong interactions. It is possible that the A783 m6A site
434 specifically is a high-affinity site for YTHDC1 interaction based on our *in vitro* analysis where YTHDC1
435 association with methylated domain 2 of HOTAIR was dependent on this site (Figure 5A-C). In line with
436 this hypothesis, we observe a decrease in chromatin-association when A783 of HOTAIR is mutated,
437 which is recovered upon overexpression or direct tethering of YTHDC1 (Figures 5 and 6).

438 While it is evident that m6A modification of A783 in HOTAIR is important for mediating its effects
439 in breast cancer, other m6A sites within HOTAIR appear to play a role in enabling its high expression
440 levels, potentially through transcript stabilization. When we bypass the normal mechanism of chromatin
441 association using a direct tethering approach for HOTAIR (Figure 7A)(Portoso et al., 2017), YTHDC1 is
442 no longer required for chromatin association or stability, yet is required for gene repression, suggesting
443 a direct role in shutting down transcription, perhaps with LSD1 involvement(Jarroux et al., 2021; Tsai et
444 al., 2010). Our work emphasizes the importance of studying the function of individual m6A sites, as each
445 m6A site has the potential to contribute to the function of an RNA in different ways.

446 m6A in gene repression and heterochromatin formation

447 HOTAIR and other lncRNAs make many dynamic and multivalent interactions with proteins that
448 interact with other proteins, RNA molecules, and chromatin. In the nucleus, the METTL3/14 complex and
449 YTHDC1 are key interactors with m6A-modified RNA that have been shown to regulate chromatin. Work
450 in mouse embryonic stem cells has shown that METTL3 interacts with the SETD1B histone modifying
451 complex, and this plays a role in repression of specific families of endogenous retroviruses(Xu et al.,
452 2021). However, due to the nature of HOTAIR's mechanism of repressing genes in *trans*, it is unlikely
453 that the METTL3/14 complex remains bound to HOTAIR to induce repression of target loci. For YTHDC1,
454 recent work has found that RNA interactions with this protein can directly regulate chromatin via
455 recruitment of KDM3B, promoting H3K9me2 demethylation and gene expression (Y. Li et al., 2020). In
456 contrast, this study demonstrates that YTHDC1 can act to regulate chromatin association and
457 transcriptional repression by HOTAIR, although the mechanism by which this is accomplished remains
458 ambiguous. Our data suggest that YTHDC1-mediated transcriptional repression occurs upstream of
459 chromatin modification by PRC2. This supports the mechanism of transcriptional interference by HOTAIR
460 proposed by Portoso et. al.(Portoso et al., 2017) (Figure 1A) and suggests that YTHDC1 is an important
461 factor that mediates repression by HOTAIR. Yet, it is still unclear how YTHDC1 binding to a repressive
462 lncRNA mediates transcriptional interference and repression.

463 Divergence in m6A and YTHDC1 function for different classes of RNAs

464 The role of YTHDC1 in mediating chromatin association of and repression by HOTAIR is
465 interesting in the context of the recently identified broad nuclear role of YTHDC1 in regulation of
466 transcription and chromatin state in mouse embryonic stem cells(Jun Liu et al., 2020). While in this case
467 it was demonstrated that YTHDC1 mediates degradation of m6A-modified chromatin-associated
468 regulatory RNAs, our work raises the possibility that YTHDC1 might also mediate transcriptional
469 repression and/or heterochromatin directly through interaction with regulatory RNAs. Our work also
470 shows that, rather than degradation of HOTAIR, m6A sites in HOTAIR mediate its high expression in
471 breast cancer via YTHDC1. An important distinction between HOTAIR and the chromatin-associated
472 regulatory RNAs investigated by Liu et. al(Jun Liu et al., 2020) is that HOTAIR regulates genes in *trans*

473 versus *cis*. Liu *et. al* found that YTHDC1 mediates degradation of *cis*-regulatory RNAs by the NEXT
474 complex to slow downstream transcription of their target genes; however, in the case of HOTAIR,
475 YTHDC1 mediates chromatin association of a *trans*-regulatory lncRNA, presumably helping it to repress
476 its target genes in *trans*. We hypothesize that chromatin association of HOTAIR stabilizes it because
477 stable retention of HOTAIR on chromatin as heterochromatin forms is likely to make it inaccessible to
478 factors that mediate its degradation. Our experiments where HOTAIR is tethered to chromatin in a
479 reporter cell line illustrates this, as knockdown of YTHDC1 did not alter the stability of HOTAIR in the
480 context where it is constitutively tethered to chromatin (Figure 6 – figure supplement 1C). It is likely that
481 YTHDC1 performs multiple functions within the nucleus, and that its effects on its target RNAs are context
482 dependent, such as on other nearby RNA binding proteins and/or local chromatin state.

483 Our work also highlights the fate of HOTAIR-YTHDC1 interaction which is distinctly different from
484 mRNAs whose nuclear export is mediated by YTHDC1(Roundtree *et al.*, 2017). In contrast, we show that
485 YTHDC1 mediates chromatin association of the primarily nuclear-localized HOTAIR lncRNA. Also, while
486 one specific m6A site at A783 is important for mediating chromatin association and the physiological
487 effects of HOTAIR in breast cancer, other m6A sites play a role in overall expression or stability (Figure
488 8). It is likely that the RNA context and other proteins that either interact directly with YTHDC1 or the RNA
489 molecules it binds to dictate the effects of YTHDC1 binding to its targets. Another possibility is that
490 specific modifications on YTHDC1, such as phosphorylation (which has previously been demonstrated
491 to regulate its localization)(Rafalska *et al.*, 2004), result in interactions with different types of regulatory
492 RNAs or even different m6A sites within a single RNA, ultimately leading to differing effects (i.e. stability
493 vs. chromatin association vs. degradation). Additional studies on how YTHDC1 interacts with specific
494 RNA targets, chromatin, and other proteins in the nucleus will shed light on the mechanisms of YTHDC1
495 in chromatin regulation.

496 *Antimorphic transformation of HOTAIR function via mutation of a single m6A site*

497 The antimorphic effect of mutating A783 in HOTAIR induced opposite and additional gene
498 expression changes that ultimately resulted in a less aggressive breast cancer state (Figures 1 and 2).

499 Our results show that disruption of a single m6A site can convert HOTAIR from eliciting pro- to anti-tumor
500 effects, allowing overexpression of the converted lncRNA to decrease cancer phenotypes more so than
501 depletion of the wild-type version. Understanding the mechanism behind this induction of antimorphic
502 behavior by a single nucleotide mutation and its biological implications will require future work. Altogether,
503 these findings suggest a potential therapeutic approach to oncogenic lncRNAs such as HOTAIR, where
504 disruption of RNA methylation alone has a greater impact than simple elimination of the RNA.

505 **Conclusion**

506 The context dependency of m6A function is an emerging theme. With various roles in pluripotency
507 and development and in disease states such as cancer, m6A on different RNA molecules regulates their
508 fate and functional output in different ways(Meyer et al., 2012; L. Wu, Wu, Ning, Liu, & Zhang, 2019). Our
509 work illustrates the context of three specific m6A functions: enabling chromatin association, promoting
510 high levels of lncRNA expression, and facilitating transcriptional repression. We further highlight the
511 importance of one specific m6A site within a lncRNA that contains multiple sites of modification.

512 As the only primarily nuclear m6A reader, YTHDC1 has the potential to interact with m6A-
513 containing RNA molecules at the site of transcription on chromatin. The outcome of this interaction
514 appears to be dictated by the identity of the RNA molecule (including whether it functions in *cis* or *trans*)
515 and the cell type that it occurs in, but ultimately has the potential to result in chromatin regulation. Our
516 work demonstrates the importance of YTHDC1 in mediating HOTAIR chromatin association and
517 transcriptional repression independent of PRC2, revealing a new layer of regulation by m6A at a specific
518 residue within HOTAIR. Overall, this provides insight into mechanisms of how m6A regulates HOTAIR-
519 mediated breast cancer metastasis which could ultimately lead to new treatment options (for example,
520 preventing m6A methylation at this specific site) for patients with tumors that have elevated HOTAIR
521 levels.

522

523 **Materials and Methods**

524 **Cell Culture**

525 MCF-7 cells were maintained in RPMI media (11875093, Invitrogen) and MDA-MB-231 and 293T
526 in DMEM media (MT10013CV, Fisher Scientific). Media contained 10% FBS (F2442-500ML, Sigma-
527 Aldrich) and Pen-Strep (MT30002CI, Fisher Scientific) and cells were grown under standard tissue
528 culture conditions. Cells were split using Trypsin (MT25053CI, Fisher Scientific) according to
529 manufacturer's instructions.

530 MDA-MB-231 cells overexpressing WT HOTAIR, A783U mutant HOTAIR, or Anti-Luciferase were
531 generated as previously described using retroviral transduction(Meredith et al., 2016). Stable knockdown
532 of METTL3, METTL14, WTAP, and YTHDC1 and overexpression of YTHDC1 was performed by lentivirus
533 infection of MCF-7 or MDA-MB-231 cells overexpressing HOTAIR or A783U mutant HOTAIR via Fugene
534 HD R.8 with pLKO.1-blasticidin shRNA constructs or a pLX304 overexpression construct as noted in
535 Table S3. Cells were selected with 5 µg/mL blasticidin (Life Technologies). The nontargeting shRNA
536 pLKO.1-blast-SCRAMBLE was obtained from Addgene (Catalog #26701). Two shRNAs for each target
537 were obtained and stable lentiviral transductions with the targeted shRNAs and the scramble control were
538 performed. Cell lines with the most efficient knockdown as determined by western blot were selected for
539 downstream experiments.

540 **Plasmid Construction**

541 The pBABE-puro retroviral vector was used for overexpression of lncRNAs. The spliced HOTAIR
542 transcript (NR_003716.3) was synthesized and cloned into the pBABE-puro retroviral vector by
543 GenScript. An antisense transcript of the firefly luciferase gene (AntiLuc) was amplified from the pTRE3G-
544 Luciferase plasmid (Clonetech), then cloned into the pBABE-puro retroviral vector. These were generated
545 in a previous publication(Meredith et al., 2016).

546 To create the A783U mutant HOTAIR overexpression plasmid, staggered QuikChange oligos
547 AG66/AG67 were used to generate the A783U mutation in pTRE3G-HOTAIR using the QuikChange Site
548 Directed Mutagenesis Kit (Agilent 200519) to generate pTRE3G-A783U_HOTAIR. A 1.6Kb fragment of

549 A783U mutant HOTAIR was amplified with primers AG68/AG69 from pTRE3G-A783U_HOTAIR for
550 cloning into pBABE-Puro-HOTAIR cut with XcmI and BamHI by Gibson Assembly. Oligonucleotide
551 sequences are noted in Table S4. All constructs were confirmed by sequencing. pBABE-Puro-
552 6xAU_HOTAIR and pBabe-Puro-14xAU_HOTAIR were synthesized and cloned by GenScript.

553 Plasmids for the knockdown of METTL3, METTL14, WTAP, and YTHDC1 were generated by
554 cloning the shRNA (RNAi Consortium shRNA Library) from pLKO.1-puro into the pLKO.1-blast backbone
555 (Addgene #26655).

556 To generate the plasmid for tethering YTHDC1 to HOTAIR via dCasRX, we first constructed a
557 pCDNA-FLAG plasmid by inserting a 5xFLAG sequence (synthesized as a gBlock by IDT DNA) into the
558 HindIII/XbaI site of pCDNA3 (Invitrogen). YTHDC1 was then amplified from pLX304-YTHDC1 (ORF clone
559 ccsdBroad304_04559) with oligonucleotides noted in Table S4, and cloned into the KpnI/NotI site of
560 pCDNA-FLAG to generate pCDNA-FLAG-YTHDC1 (pAJ367). The FLAG-YTHDC1 sequence was
561 amplified then cloned downstream of dCasRX at NheI in the pXR002 plasmid (pXR002: EF1a-dCasRx-
562 2A-EGFP was a gift from Patrick Hsu (Addgene plasmid # 109050; <http://n2t.net/addgene:109050>;
563 RRID:Addgene_109050)) using oligonucleotides noted in Table S4. Expression of the dCasRX-YTHDC1
564 fusion protein was confirmed by transfection of the plasmid followed by Western Blot with anti-FLAG M2
565 mouse monoclonal antibody (F1804, Sigma-Aldrich) and anti-YTHDC1 (14392-1-AP, Proteintech).
566 Plasmids containing guide RNAs were generated using the pXR003 backbone plasmid (pXR003: CasRx
567 gRNA cloning backbone was a gift from Patrick Hsu (Addgene plasmid # 109053;
568 <http://n2t.net/addgene:109053>; RRID:Addgene_109053)) cut with BbsI, using oligonucleotides noted in
569 Table S4. All plasmids were confirmed by sequencing.

570 **m6A enhanced crosslinking immunoprecipitation:**

571 *polyA isolation and RNA fragmentation*

572 For each experiment, approximately 100 µg of total RNA was isolated from cells with TRIzol
573 according to manufacturer's instructions. 10 µg PolyA RNA was isolated using Magnosphere® Ultrapure

574 mRNA Purification Kit (Takara) according to manufacturer's instructions. PolyA RNA was ethanol
575 precipitated with 2.5 M Ammonium Acetate and 70% ethanol in a solution containing 50 µg/ml GlycoBlue
576 Co-precipitant (AM9515, Invitrogen). RNA was resuspended in 10 µl and fragmented with 10x
577 Fragmentation Buffer (AM8740, Invitrogen) at 75°C for 8 minutes and immediately quenched with 10x
578 Stop Reagent (AM8740, Invitrogen) and placed on ice to generate fragments 30-150 nucleotides in
579 length.

580 *Anti-m6A-RNA crosslinking and bead conjugation*

581 Crosslinked RNA-Antibody was generated as previously described(Grozhik, Linder, Olarerin-
582 George, & Jaffrey, 2017). Fragmented RNA was resuspended in 500 µl Binding/Low Salt Buffer (50 mM
583 Tris-HCl pH 7.4, 150 mM Sodium Chloride, 0.5% NP-40) containing 2 µl RNase Inhibitor (M0314, NEB)
584 and 10 µl m6A antibody (ab151230, Abcam), and incubated for 2 hours at room temperature with rotation.
585 RNA-Antibody sample was transferred to one well of a 12-well dish and placed in a shallow dish of ice.
586 Sample was crosslinked twice at 150 mJ/cm² using a Stratagene Stratalinker UV Crosslinker 1800 and
587 transferred to a new tube. 50 µl Protein A/G Magnetic Beads (88803, Pierce) were washed twice with
588 Binding/Low Salt Buffer, resuspended in 100 µl Binding/Low Salt Buffer, and added to crosslinked RNA-
589 Antibody sample. Beads were incubated at 4°C overnight with rotation.

590 *eCLIP library preparation*

591 RNA was isolated and sequencing libraries were prepared using a modified enhanced CLIP
592 protocol(Van Nostrand et al., 2016). Beads were washed twice with High Salt Wash Buffer (50 mM Tris-
593 HCl pH 7.4, 1 M Sodium Chloride, 1 mM EDTA, 1% NP-40, 0.5% Sodium Deoxycholate, 0.1% Sodium
594 Dodecyl Sulfate), once with Wash Buffer (20 mM Tris-HCl pH 7.4, 10 mM Magnesium Chloride, 0.2%
595 Tween-20), once with Wash Buffer and 1x Fast AP Buffer (10 mM Tris pH 7.5, 5 mM Magnesium Chloride,
596 100 mM Potassium Chloride, 0.02% Triton X-100) combined in equal volumes, and once with 1x Fast AP
597 Buffer. Beads were resuspended in Fast AP Master Mix (1x Fast AP Buffer containing 80U RNase
598 Inhibitor (M0314, NEB), 2U TURBO DNase (AM2238, Invitrogen), and 8U Fast AP Enzyme (EF0654,
599 Thermo Scientific)) was added. Samples were incubated at 37°C for 15 minutes shaking at 1200 rpm.

600 PNK Master Mix (1x PNK Buffer (70 mM Tris-HCl pH 6.5, 10 mM Magnesium Chloride), 1 mM
601 Dithiothreitol, 200U RNase Inhibitor, 2U TURBO DNase, 70U T4 PNK (EK0031, Thermo Scientific)) was
602 added to the samples and they incubated at 37°C for 20 minutes shaking at 1200 rpm.

603 Beads were washed once with Wash Buffer, twice with Wash Buffer and High Salt Wash Buffer
604 mixed in equal volumes, once with Wash Buffer, once with Wash Buffer and 1x Ligase Buffer (50 mM
605 Tris pH 7.5, 10 mM Magnesium Chloride) mixed in equal volumes, and twice with 1x Ligase Buffer. Beads
606 were resuspended in Ligase Master Mix (1x Ligase Buffer, 1 mM ATP, 3.2% DMSO, 18% PEG 8000,
607 16U RNase Inhibitor, 75U T4 RNA Ligase I (M0437, NEB)), two barcoded adaptors were added (X1a
608 and X1b, see Table S5), and samples were incubated at room temperature for 75 minutes with flicking
609 every 10 minutes. Beads were washed once with Wash Buffer, once with equal volumes of Wash Buffer
610 and High Salt Wash Buffer, once with High Salt Wash Buffer, once with equal volumes of High Salt Wash
611 Buffer and Wash Buffer, and once with Wash Buffer. Beads were resuspended in Wash Buffer containing
612 1x NuPAGE LDS Sample Buffer (NP0007, Invitrogen) and 0.1M DTT, and incubated at 70°C for 10
613 minutes shaking at 1200 rpm.

614 Samples were cooled to room temperature and supernatant was ran on Novex NuPAGE 4-12%
615 Bis-Tris Gel (NP0321, Invitrogen). Samples were transferred to nitrocellulose membrane, and
616 membranes were cut and sliced into small pieces between 20 kDa and 175 kDa to isolate RNA-antibody
617 complexes. Membrane slices were incubated in 20% Proteinase K (03508838103, Roche) in PK Buffer
618 (100 mM Tris-HCl pH 7.4, 50 mM NaCl, 10 mM EDTA) at 37°C for 20 minutes shaking at 1200 rpm. PK
619 Buffer containing 7M urea was added to samples and samples were incubated at 37°C for 20 minutes
620 shaking at 1200 rpm. Phenol:Chloroform:Isoamyl Alcohol (25:24:1) (P2069, Sigma-Aldrich) was added
621 to samples and samples were incubated at 37°C for 5 minutes shaking at 1100 rpm. Samples were
622 centrifuged 3 minutes at 16,000 x g and aqueous layer was transferred to a new tube.

623 RNA was isolated using RNA Clean & Concentrator-5 Kit (R1016, Zymo) according to
624 manufacturer's instructions. Reverse transcription was performed using AR17 primer (Table S5) and
625 SuperScript IV Reverse Transcriptase (18090010, Invitrogen). cDNA was treated with ExoSAP-IT

626 Reagent (78201, Applied Biosystems) at 37°C for 15 minutes, followed by incubation with 20 mM EDTA
627 and 0.1M Sodium Hydroxide at 70°C for 12 minutes. Reaction was quenched with 0.1M Hydrochloric
628 Acid. cDNA was isolated using Dynabeads MyONE Silane (37002D, ThermoFisher Scientific) according
629 to manufacturer's instructions. 20% DMSO and rand3Tr3 adaptor (Table S5) was added to samples, and
630 samples were incubated at 75° for 2 minutes. Samples were placed on ice and Ligation Master Mix (1x
631 NEB Ligase Buffer, 1mM ATP, 25% PEG 8000, 15U T4 RNA Ligase I (NEB)) was added to samples.
632 Samples were mixed at 1200 rpm for 30 seconds prior to incubation at room temperature overnight.

633 cDNA was isolated using Dynabeads MyONE Silane according to manufacturer's instructions and
634 eluted with 10 mM Tris-HCl pH 7.5. A 1:10 dilution of cDNA was used to quantify the cDNA library by
635 qPCR using a set of Illumina's HT Seq primers, and Ct values were used to determine number of cycles
636 for PCR amplification of cDNA. The undiluted cDNA library was amplified by combining 12.5µL of the
637 sample with 25µL Q5 Hot Start PCR Master Mix and 2.5µL (20µM) of the same indexed primers used
638 previously. Amplification for the full undiluted sample used 3 cycles less than the cycle selected from the
639 diluted sample. The PCR reaction was isolated using HighPrep PCR Clean-up System (AC-60050,
640 MAGBIO) according to manufacturer's instructions.

641 The final sequencing library was gel purified by diluting the sample with 1x Orange G DNA loading
642 buffer and running on a 3% quick dissolve agarose gel containing SYBR Safe Dye (1:10,000). Following
643 gel electrophoresis, a long wave UV lamp was used to extract DNA fragments from the gel ranging from
644 175 to 300 base pairs. The DNA was isolated using QiaQuick MinElute Gel Extraction Kit (28604,
645 Qiagen). The purified sequencing library was analyzed via TapeStation using DNA ScreenTape (either
646 D1000 or HS D1000) according to the manufacturer's instructions to assess for appropriate size and
647 concentration (the final library should be between 175 and 300 base pairs with an ideal concentration of
648 at least 10nM).

649 *Sequencing and analysis*

650 Samples were sequenced at the Genomics and Microarray Shared Resource facility at University
651 of Colorado Denver Cancer Center on an Illumina MiSeq or NovaSEQ6000 with 2x 150 base pair paired-

652 end reads to generate 40 million raw reads for each sample. Computational analysis methods are
653 described in (Roberts et al., 2020). Briefly, a custom Snakemake workflow was generated based on the
654 original eCLIP analysis strategies(Van Nostrand et al., 2016) to map reads to the human genome. To
655 identify m6A sites, we used a custom analysis pipeline to identify variations from the reference genome
656 at single-nucleotide resolution across the entire genome. We then employed an internally developed Java
657 package to identify C-to-T mutations occurring 1) within the m⁶A consensus motif 'RAC': 'R' is any purine,
658 A or G; A being the methylated adenosine; and C where the mutation occurs; and 2) within a frequency
659 range of greater than or equal to 2.5% and less than or equal to 50% of the total reads at a given position
660 (with a minimum of 3 C-to-T mutations at a single site). The resulting m⁶A sites were then compared to
661 those identified in the corresponding input sample and any sites occurring in both were removed from
662 the final list of m⁶A sites (this eliminates any mutations that are not directly induced from the anti-m⁶A
663 antibody crosslinking). Full transcriptome data associated with the methods manuscript(Roberts et al.,
664 2020) is at GEO accession number GSE147440.

665 **m6A RNA Immunoprecipitation (meRIP)**

666 Total RNA was isolated with TRIzol (15596018, Invitrogen) according to the manufacturer's
667 instructions. RNA was diluted to 1 µg/µl and fragmented with 1x Fragmentation Buffer (AM8740,
668 Invitrogen) at 75°C for 5 minutes. 1x Stop Reagent (AM8740, Invitrogen) was added immediately
669 following fragmentation and samples placed on ice. 500 ng of input sample was reserved in 10 µl
670 nuclease free water for qRT-PCR normalization. Protein A/G Magnetic Beads (88803, Pierce) were
671 washed twice with IP Buffer (20 mM Tris pH 7.5, 140 mM NaCl, 1% NP-40, 2mM EDTA) and coupled
672 with anti-m6A antibody (ab151230, Abcam) or an IgG control (NB810-56910, Novus) for 1 hour at room
673 temperature. Beads were washed 3 times with IP Buffer. 10 µg fragmented RNA and 400U RNase
674 inhibitor was added to 1 ml IP Buffer. Antibody-coupled beads were resuspended in 500 µl RNA mixture
675 and incubated 2 hours to overnight at 4°C on a rotor. Beads were washed 5 times with cold IP Buffer.
676 Elution Buffer (1x IP Buffer containing 10 U/µl RNase inhibitor and 0.5 mg/ml N6-methyladenosine 5'-
677 monophosphate (M2780, Sigma-Aldrich) was prepared fresh and kept on ice. Samples were eluted with

678 200 μ l Elution Buffer for 2 hours at 4°C on a rotor. Supernatant was removed and ethanol precipitated
679 with 2.5M Ammonium Acetate, 70% Ethanol, and 50 μ g/ml GlycoBlue Coprecipitant (Invitrogen AM9515).
680 RNA was washed with 70% ethanol, dried for 10 minutes at room temperature, and resuspended in 10
681 μ l nuclease free water. RNA was quantified by nanodrop and 200 ng RNA was reverse transcribed using
682 High Capacity cDNA Reverse Transcription Kit (4368814, ThermoFisher Scientific) and quantified by
683 qPCR (oligonucleotides listed in Table S6), and fraction recovered was calculated from Input and IP
684 values.

685 **RNA Immunoprecipitation of YTHDC1**

686 Actively growing cells from 70-90% confluent 15-cm dishes were trypsinized and washed twice
687 with ice-cold 1x PBS. Cell pellet was resuspended in 1% V/V Formaldehyde (28908, Pierce) in 1x PBS
688 and incubated at room temperature for 10 minutes on a rotor. Crosslinking was quenched with 0.25 M
689 glycine at room temperature for 5 minutes. Cells were washed 3 times with ice-cold 1x PBS and placed
690 on ice. 20 μ l Protein A/G beads were washed twice with RIPA Binding Buffer (50 mM Tris-HCl pH 7.4,
691 100 mM Sodium Chloride, 1% NP-40, 0.1% Sodium Dodecyl Sulfate, 0.5% Sodium Deoxycholate, 4 mM
692 Dithiothreitol, 1x Protease Inhibitors), resuspended in 1 ml RIPA Binding Buffer, and split to two 0.5 ml
693 aliquots. 2 μ g YTHDC1 antibody (ab122340, Abcam) or an IgG Control (sc-2027, Santa Cruz
694 Biotechnology) was added to beads and incubated for 2 hours at 4°C on a rotor. Fixed cells were
695 resuspended in 1 ml RIPA Binding Buffer and placed in the Bioruptor Pico (B01060010, Diagenode) for
696 10 cycles of 30 seconds on, 30 seconds off. Lysates were digested with TURBO DNase for 5 minutes at
697 37°C with mixing at 1000 rpm and transferred to ice for 5 minutes. Lysates were clarified by centrifugation
698 at 17,000g at 4°C for 10 minutes and supernatant was transferred to a new tube. 200U RNase Inhibitor
699 was added to the 1 ml clarified lysate. A 5% aliquot was removed and processed downstream with IP
700 samples. A 2% aliquot was removed and diluted with 1x SDS Sample Buffer (62.5 mM Tris-HCl pH 6.8,
701 2.5% SDS, 0.002% Bromophenol Blue, 5% β -mercaptoethanol, 10% glycerol) and protein input and
702 recovery was monitored by Western Blot. Antibody-coupled beads were washed 3 times with RIPA
703 Binding Buffer and resuspended in half of the remaining lysate. Samples were incubated overnight at

704 4°C on a rotor. Beads were washed 5 times with RIPA Wash Buffer (50 mM Tris-HCl pH 7.4, 1 M Sodium
705 Chloride, 1% NP-40, 0.1% Sodium Dodecyl Sulfate, 0.5% Sodium Deoxycholate, 1 M Urea, 1x Protease
706 Inhibitors) and resuspended in 100 µl RNA Elution Buffer (50 mM Tris-HCl pH 7.4, 5 mM EDTA, 10 mM
707 Dithiothreitol, 1% Sodium Dodecyl Sulfate). Input sample was diluted with 1x RNA Elution Buffer.
708 Formaldehyde crosslinks in both input and IP samples were reversed by incubation at 70°C for 30
709 minutes at 1000 rpm. Supernatant was transferred to a new tube and RNA was isolated using TRIzol-LS
710 according to the manufacturer's instructions. Reverse transcription was performed on 100 ng RNA using
711 SuperScript IV Reverse Transcriptase. qPCR was performed as described below.

712 **RNA Isolation and qRT-PCR**

713 RNA was isolated with TRIzol (Life Technologies) with extraction in chloroform followed by
714 purification with the RNeasy kit (Qiagen). Samples were DNase treated using TURBO DNase (Ambion).
715 Reverse transcription was performed using the cDNA High Capacity Kit (Life Technologies). qPCR was
716 performed using Sybr Green master mix (Takyon, AnaSpec Inc.) using the primers listed in Table S6 on
717 a C1000 Touch Thermocycler (BioRad). EEF1A1 primer sequences were obtained from the Magna
718 MeRIP m6A kit (17-10499, Sigma-Aldrich). Sequences for Luciferase primers (LucR2) were obtained
719 from a previous publication(Vaquero et al., 2004). Three qPCR replicates were performed for each
720 sample, and these technical replicates were averaged prior to analysis of biological replicates. At least 3
721 biological replicates were performed for each qPCR experiment.

722 **Cell Proliferation Assays**

723 Three independent clones, here defined as a pool of selected cells stably expressing the pBabe
724 plasmid, were analyzed for cell proliferation. 2,000 cells were plated in a 96-well dish in DMEM media
725 containing 10% FBS and selective antibiotics (1µg/ml puromycin (P8833, Sigma-Aldrich) and/or 5µg/ml
726 blasticidin (71002-676, VWR)), allowed to settle at room temperature for 20 minutes, then placed in an
727 Incucyte® S3 (Sartorius). Pictures were taken with a 10x magnification every 2 hours for 48 hours using
728 a Standard scan. Confluency was determined using the Incucyte ZOOM software. Growth rate was
729 calculated from % confluency using the Least Squares Fitting Method(Roth, 2006).

730 **Cell Invasion Assays**

731 MDA-MB-231 cell lines were grown to 70-90% confluence and serum starved in OptiMEM for ~20
732 hours prior to setting up the experiment. Cells were washed, trypsinized, and resuspended in 0.5% serum
733 DMEM. 10% serum DMEM was added to the bottom chamber of Corning Matrigel™ Invasion Chambers
734 (Corning 354481), and 200,000 cells were plated in the top chamber in 0.5% serum DMEM. Cells were
735 incubated for 22 hours at 37°C followed by 4% PFA fixation and 0.1% Crystal Violet staining. Matrigel
736 inserts were allowed to dry overnight, followed by brightfield imaging with a 20X air objective. Four
737 biological replicates were performed, with technical duplicates in each set. For each Matrigel insert, four
738 fields of view were captured, and cells were counted in Fiji (eight data points per condition, per biological
739 replicate). The violin plot includes all of the data points, while statistical analysis was performed on the
740 average number of cells/field for each biological replicate.

741 **Gene Expression Analyses**

742 Total RNA was extracted from MDA-MB-231 cells using TRIzol (Life Technologies) with extraction
743 in chloroform followed by purification with the RNeasy kit (Qiagen). Samples were DNase treated using
744 TURBO DNase (Ambion). polyA-selected sequencing libraries were prepared and sequenced by The
745 Genomics Shared Resource at the University of Colorado Cancer Center. All gene expression data
746 associated with this publication is available through GEO accession number GSE173530. Differential
747 gene expression analysis was performed using Salmon and DESeq2(Love, Huber, & Anders, 2014;
748 Patro, Duggal, Love, Irizarry, & Kingsford, 2017). Briefly, the reads were quantified using salmon to
749 generate transcript abundance estimates and then DESeq2 was used to determine differential expression
750 between samples. Heat maps were generated by using normalized read counts of genes that were
751 significantly ($p<0.1$) differentially expressed between conditions to generate Z-scores. GO term
752 enrichment analysis was performed using the GO Consortium's online PANTHER tool(Ashburner et al.,
753 2000; Mi, Muruganujan, Ebert, Huang, & Thomas, 2019; "The Gene Ontology resource: enriching a GO
754 mine.," 2021). To analyze correlation between expression in HOTAIR v. Control and A783U v. Control
755 pairwise comparisons, the total set of differentially expressed genes were filtered to include only those

756 whose fold change value was greater than 1.15 in either direction for both comparisons. These values
757 were then plotted against each other. Linear regression was used to fit a trend line over the points, with
758 the calculated Pearson correlation coefficient included in the graph.

759 **Purification of METTL3/14**

760 Suspension-adapted HEK293 cells (Freestyle™ 293-F cells, R790-07, Life Technologies) were
761 grown as recommended in Freestyle™ 293 Expression Medium (12338026, Life Technologies,) sharking
762 at 37°C in 5% CO₂. Cells were grown to a concentration of 3 x 10⁶ cells/ml and diluted to 1 x 10⁶ cells/ml
763 in 50 ml 293F Freestyle Media 24 hours prior to transfection. Before transfection, cells were spun down
764 and resuspended in 50 ml fresh 293F Freestyle Media at a concentration of 2.5 x 10⁶ cells/ml. Expression
765 plasmid (pcDNA3.1-FLAG-METTL3, pcDNA3.1-FLAG-METTL14) were added to the flask at a
766 concentration of 1.5 µg, and flask was shaken in the incubator for 5 minutes. 9 µg/ml PEI was added to
767 the flask and cells were returned to incubator. After 24 hours of growth, an additional 50 ml fresh 293F
768 Freestyle Media was added and culture was supplemented with 2.2 mM VPA. Cells were harvested as
769 two 50 ml pellets 72 hours after addition of VPA.

770 Cell pellets were resuspended in 1x Lysis Buffer (50 mM Tris pH 7.4, 150 mM Sodium Chloride,
771 1 mM EDTA, 1% TritonX-100, 1x Protease inhibitors) to obtain a concentration of 10⁷ cells/ml and
772 incubated for 20 minutes at 4°C with rotation. Cell lysate was clarified by centrifugation at 4°C, 12,000 x
773 g for 15 minutes. Supernatant was transferred to a new tube and kept on ice. Anti-FLAG M2 affinity resin
774 was equilibrated with 1x Lysis Buffer by washing 3 times. Equilibrated resin was resuspended in 1x Lysis
775 Buffer and added to the tube containing the clarified lysate. Sample was incubated for 2 hours at 4°C
776 with rotation. Resin was pelleted by centrifugation at 4°C, 500 x g. Supernatant was removed, and resin
777 was washed 3 times with 1x Wash Buffer (50 mM Tris pH 7.4, 150 mM Sodium Chloride, 10% Glycerol,
778 1 mM Dithiothreitol) for 5 minutes each at 4°C with rotation. Sample was equilibrated to room temperature
779 and resin was resuspended in 1x Wash Buffer containing 0.2 mg/ml 3xFLAG Peptide. Samples were
780 incubated at room temperature for 10 minutes shaking at 1000 rpm, centrifuged for 2 minutes at 1000 x
781 g, and supernatant was reserved (elution 1). Elution was repeated twice to obtain two additional elution

782 samples (elution 2 and 3). Samples were analyzed by Coomassie to determine protein concentration and
783 purity. Samples were aliquoted and stored at -80°C and thawed on ice prior to use in *in vitro* m6A
784 methylation experiments.

785 ***In vitro* m6A methylation and interaction assays**

786 All plasmids and oligonucleotides used in this assay are listed in Table S7. Using PCR, we
787 generated a DNA fragment for Domain 2 of wild-type (pTRE3G-HOTAIR, pAJ171) and A783U (pTRE3G-
788 A783U_HOTAIR, pAJ385) mutant HOTAIR using primers MB88 and MB89. A 5' T7 promoter and 3' RAT
789 tag were added to the sequence via PCR with primers MB22 and MB94. *in vitro* transcription of the PCR
790 templates was completed using the MEGAScript T7 Transcription Kit (AM1334, ThermoFisher Scientific)
791 according to the manufacturer's instructions, and RNA was purified using the RNeasy Mini Kit (Qiagen
792 75106). 500 nM RNA was diluted in 1x Methyltransferase Buffer (20 mM Tris pH 7.5, 0.01% Triton-X 100,
793 1 mM DTT) in reactions containing 50 µM SAM and 500 nM purified METTL3/14 (+m6A) for 1 hour at
794 room temperature. Control reactions contained no METTL3/14 (-m6A). RNA was purified using the
795 RNeasy Mini Kit according to manufacturer's instructions.

796 To obtain FLAG-tagged YTHDC1 protein, 293 cells were transfected using Lipofectamine 2000
797 (11668030, ThermoFisher Scientific) with plasmid YTHDC1-FLAG and cell lysates were generated as
798 previously described(Meredith et al., 2016). Dynabeads (M270, Invitrogen) were resuspended in high-
799 quality dry Dimethylformamide at a concentration of 2×10^9 beads/ml. Dynabeads were stored at 4°C
800 and equilibrated to room temperature prior to use. Dynabeads were washed in 0.1 M Sodium Phosphate
801 Buffer (pH 7.4) and vortexed for 30 seconds. A second wash was repeated with vortexing and incubation
802 at room temperature for 10 minutes with rotation. 1 mg/ml IgG solution was prepared by diluting rabbit
803 IgG (15006, Sigma) in 0.1 M Sodium Phosphate Buffer. Washed beads were resuspended in 0.1 M
804 Sodium Phosphate Buffer at a concentration of 3×10^9 beads/ml, and an equal volume of 1 mg/ml IgG
805 was added. Samples were vortexed briefly and an equal volume of 3M Ammonium Sulfate was added
806 and samples were mixed well. Samples were incubated at 37°C for 18-24 hours with rotation. Samples
807 were washed once briefly with 0.1 M Sodium Phosphate Buffer, then twice with incubation at room

808 temperature for 10 minutes with rotation. Samples were washed in Sodium Phosphate Buffer + 1%
809 TritonX-100 at 37°C for 10 minutes with rotation. A quick wash with 0.1 M Sodium Phosphate Buffer was
810 performed and followed by 4 washes in 0.1 M Citric Acid pH 3.1 at a concentration of 2×10^8 beads/ml
811 at room temperature for 10 minutes with rotation. After a quick wash with 0.1 M Sodium Phosphate Buffer,
812 beads were resuspended to 1×10^9 beads/ml in 1x PBS + 0.02% Sodium Azide and stored at 4°C prior
813 to use.

814 800 ng of +/-m6A RNA was incubated with 150 ng PrA-PP7 fusion protein in HLB300 (20 mM
815 Hepes pH 7.9, 300 mM sodium chloride, 2 mM magnesium chloride, 0.1% NP-40, 10% glycerol, 0.1 mM
816 PMSF, 0.5 mM DTT). RNA was prebound to PP7 for 30 minutes at 25°C, 1350 rpm. 75 μ l IgG-coupled
817 Dynabeads were washed with HLB300 twice and resuspended in 250 μ l HLB300. 50 μ l beads were
818 added to each tube of RNA-PP7 and samples were incubated 1 hour at 25°C, 1350 rpm. Beads were
819 washed twice with HLB300 and resuspended in 80 μ l Binding Buffer (10 mM Hepes pH 7.4, 150 mM
820 potassium chloride, 3 mM magnesium chloride, 2 mM DTT, 0.5% NP-40, 10% glycerol, 1mM PMSF, 1x
821 protease inhibitors) containing 80U RNase Inhibitor. 25 μ g YTHDC1-FLAG containing lysate and 800 ng
822 competitor RNA (IVT untagged HOTAIR D2) was added to each sample. Samples were incubated at 4°C
823 for 2.5 hours on a rotor. Beads were washed 3 times with cold Wash Buffer (200 mM Tris-HCl pH 7.4,
824 200 mM sodium chloride, 2 mM magnesium Chloride, 1 mM DTT, 1x protease inhibitors) and
825 resuspended in 1x SDS loading buffer. A 10% protein input sample was diluted in 1x SDS loading buffer.
826 Samples were boiled 5 minutes at 95°C and supernatant transferred to a new tube. Half of each sample
827 was loaded on a 10% acrylamide gel and Western Blot was performed using anti-FLAG antibody.

828 **Fractionation**

829 Cells were grown in 15-cm dishes to 70-90% confluency. Cells were released with Trypsin
830 (Corning), washed once with 1x PBS containing 1 mM EDTA, and split into two volumes. 1/4 of the
831 sample was harvested in TRIzol and RNA isolated with RNeasy kit for the input RNA sample. The
832 remaining 3/4 of the sample was fractionated into cytoplasmic, nucleoplasmic, and chromatin-associated
833 samples. Cells were lysed in cold Cell Lysis Buffer (10 mM Tris-HCl pH 7.5, 0.15% NP-40, 150 mM

834 Sodium Chloride) containing RNase inhibitors for 5 minutes on ice. Lysate was layered onto 2.5 volumes
835 of Sucrose Cushion (10mM Tris-HCl pH7.5, 150 mM Sodium Chloride, 24% Sucrose) containing RNase
836 inhibitors. Samples were centrifuged for 10 minutes at 17,000xg at 4°C. Supernatant was collected
837 (Cytoplasmic sample). Pellet was rinsed with 1x PBS containing 1 mM EDTA and resuspended in cold
838 Glycerol Buffer (20 mM Tris-HCl pH 7.9, 75 mM Sodium Chloride, 0.5 mM EDTA, 0.85 mM DTT, 0.125
839 mM PMSF, 50% Glycerol) containing RNase inhibitors. An equal volume of cold Nuclei Lysis Buffer (10
840 mM HEPES pH 7.6, 1 mM DTT, 7.5 mM Magnesium Chloride, 0.2 mM EDTA, 0.3 M Sodium Chloride,
841 1M Urea, 1% NP-40) was added and sample was briefly vortexed twice for 2 seconds. Samples were
842 incubated on ice 2 minutes and centrifuged for 2 minutes at 17,000xg at 4°C. Supernatant was collected
843 (Nucleoplasmic sample). The remaining pellet was resuspended in 1x PBS containing 1 mM EDTA
844 (Chromatin-associated sample). Each sample was subjected to TURBO DNase digestion at 37°C for 30
845 minutes in 1x TURBO Buffer and 10 U TURBO for cytoplasmic and nucleoplasmic samples, or 40U
846 TURBO for chromatin-associated sample. Reactions were quenched with 10mM EDTA and 3 volumes
847 of TRIzol-LS was added. RNA isolation was performed as recommended by manufacturer. Samples were
848 quantified by nanodrop to determine RNA concentration and ran on a 2% agarose gel to confirm RNA
849 integrity. qRT-PCR was performed on 2 µg of RNA and normalized to RNA recovery, input values, and
850 GAPDH.

851 **dCasRX-YTHDC1 and gRNA Transfection**

852 One plasmid containing dCasRX-FLAG-YTHDC1 in pXR002 in combination with one plasmid
853 containing the designated guide RNA in pXR003 (see description in Plasmid Construction) were
854 transfected into a 70-90% confluent 10-cm dish using Lipofectamine 2000 (11668030, Invitrogen)
855 according to manufacturer's instructions. Plates were incubated at 37°C for ~24 hours, then subjected to
856 fractionation as described above.

857 **siRNA Transfection**

858 Silencer Select siRNAs were obtained from ThermoFisher targeting YTHDC1 (n372360,
859 n372361, n372362) or Negative Controls (4390843, 4390846) and transfected into 293 cell lines using

860 Lipofectamine RNAiMAX Transfection Reagent (13778030, ThermoFisher). Transfections were
861 performed in a 24-well plate with 5 pmol of siRNA and 1.5 μ l RNAiMAX Transfection reagent per well.
862 Cells were harvested 24 hours after transfections and analyzed by Luciferase Assay and qRT-PCR.

863 **Luciferase Assay**

864 Analysis of luciferase activity was performed using the Luciferase Assay System (E1500,
865 Promega). Cells were washed with 1x PBS and lysed in 100 μ l 1x Cell Culture Lysis Reagent. Cells were
866 scraped from bottom of dish and suspension was transferred to a new tube. Lysates were frozen and
867 thawed prior to luciferase assay to ensure complete lysis. Luciferase assays were performed on 20 μ l of
868 lysate or 1x Cell Culture Lysis Reagent in 96 well plates on the GloMax-Multi Detection System (TM297,
869 Promega). 100 μ l Luciferase Assay Reagent was added to wells, mixed, and light production measured.
870 Measurements were performed in 3 technical replicates for each biological replicate. Luciferase activity
871 was normalized to protein concentration of samples.

872 **Statistical Analyses**

873 Graphs were prepared and data fitting and statistical analyses were performed using Biovinci \circledcirc
874 (version 1.1.5, Bioturing, Inc., San Diego, California, USA). Each box-and-whisker plot displays
875 datapoints for each replicate, the median value as a line, a box around the lower and upper quartiles,
876 and whiskers extending to maximum and minimum values, excluding outliers as determined by the upper
877 and lower fences. A student's unpaired T-test was used to determine statistical significance. Differences
878 and relationships were considered statistically significant when $p \leq 0.05$. For all graphs, * $p < 0.05$, ** $p <$
879 0.01, *** $p < 0.001$, **** $p < 0.0001$.

880

881

882 **Acknowledgements**

883 This work was funded by the NIH (R35GM119575 (AMJ), R01CA187733 (JKR), T32CA190216 (AMP),
884 T32GM008730 (JTR), F31CA247343 (JTR), F32CA239436 (MMW), and NCI Cancer Center Support

885 Grant P30CA046934 to the University of Colorado Cancer Center), a Department of Defense Breast
886 Cancer Research Program Fellowship Award BC170270 (AMP), and an RNA Bioscience Initiative Grant.
887 We thank Maggie M. Balas for figure advice and preparation, Rafael Margueron for providing MS2-
888 tethered HOTAIR cell lines used in this study, Chuan He for providing METTL3 and METTL14 expression
889 plasmids, Patrick Hsu for providing the dCasRX plasmids, and John Rinn, Suja Jagannathan, Neelanjan
890 Mukherjee, and Maria Aristizabal for their suggestions on the manuscript.

891

892 **Author Contributions**

893 AMP, JTR, JKR, and AMJ designed research; AMP, JTR, MC, EDD, AL, MK performed experiments;
894 AMP, JTR, and MMW analyzed data; and AMP, JKR, and AMJ wrote the paper.

895

896 **Competing Interests**

897 The authors declare that they have no competing interests.

898

899

900

901 **References**

902 Alarcon, C. R., Goodarzi, H., Lee, H., Liu, X., Tavazoie, S., & Tavazoie, S. F. (2015). HNRNPA2B1 Is a
903 Mediator of m(6)A-Dependent Nuclear RNA Processing Events. *Cell*, 162(6), 1299–1308.
904 <https://doi.org/10.1016/j.cell.2015.08.011>

905 Arshi A, Raeisi F, Mahmoudi E, Mohajerani F, Kabiri H, Fazel R, Zabihian-Langeroudi M, J. A. (2020).
906 A comparative study of HOTAIR expression in breast cancer patient tissues and cell lines. *Cell J*,
907 22(2), 178–184. <https://doi.org/10.22074/cellj.2020.6543>

908 Ashburner, M., Ball, C. A., Blake, J. A., Botstein, D., Butler, H., Cherry, J. M., ... Sherlock, G. (2000).
909 Gene ontology: tool for the unification of biology. The Gene Ontology Consortium. *Nature
910 Genetics*, 25(1), 25–29. <https://doi.org/10.1038/75556>

911 Balas, M. M., & Johnson, A. M. (2018). Exploring the mechanisms behind long noncoding RNAs and
912 cancer. *Non-Coding RNA Research*, 3(3), 108–117. <https://doi.org/10.1016/j.ncrna.2018.03.001>

913 Chandrashekhar, D. S., Bashel, B., Balasubramanya, S. A. H., Creighton, C. J., Ponce-Rodriguez, I.,
914 Chakravarthi, B. V. S. K., & Varambally, S. (2017). UALCAN: A Portal for Facilitating Tumor
915 Subgroup Gene Expression and Survival Analyses. *Neoplasia*, 19(8), 649–658.
916 <https://doi.org/https://doi.org/10.1016/j.neo.2017.05.002>

917 Coker, H., Wei, G., & Brockdorff, N. (2019). m6A modification of non-coding RNA and the control of
918 mammalian gene expression. *Biochimica et Biophysica Acta. Gene Regulatory Mechanisms*,
919 1862(3), 310–318. <https://doi.org/10.1016/j.bbagr.2018.12.002>

920 Coker, H., Wei, G., Moindrot, B., Mohammed, S., Nesterova, T., & Brockdorff, N. (2020). The role of the
921 Xist 5' m6A region and RBM15 in X chromosome inactivation. *Wellcome Open Research*, 5, 31.
922 <https://doi.org/10.12688/wellcomeopenres.15711.1>

923 Deng, J., Yang, M., Jiang, R., An, N., Wang, X., & Liu, B. (2017). Long Non-Coding RNA HOTAIR
924 Regulates the Proliferation, Self-Renewal Capacity, Tumor Formation and Migration of the Cancer
925 Stem-Like Cell (CSC) Subpopulation Enriched from Breast Cancer Cells. *PLOS ONE*, 12(1),
926 e0170860. Retrieved from <https://doi.org/10.1371/journal.pone.0170860>

927 Esteller, M. (2011). Non-coding RNAs in human disease. *Nature Reviews Genetics*, 12(12), 861–874.
928 <https://doi.org/10.1038/nrg3074>

929 Grozhik, A. V., Linder, B., Olarerin-George, A. O., & Jaffrey, S. R. (2017). Mapping m(6)A at Individual-
930 Nucleotide Resolution Using Crosslinking and Immunoprecipitation (miCLIP). *Methods in
931 Molecular Biology (Clifton, N.J.)*, 1562, 55–78. https://doi.org/10.1007/978-1-4939-6807-7_5

932 Gupta, R. a, Shah, N., Wang, K. C., Kim, J., Horlings, H. M., Wong, D. J., ... Chang, H. Y. (2010). Long
933 non-coding RNA HOTAIR reprograms chromatin state to promote cancer metastasis. *Nature*,
934 464(7291), 1071–1076. <https://doi.org/10.1038/nature08975>

935 Gyorffy, B., Lanczky, A., Eklund, A. C., Denkert, C., Budczies, J., Li, Q., & Szallasi, Z. (2010). An online
936 survival analysis tool to rapidly assess the effect of 22,277 genes on breast cancer prognosis
937 using microarray data of 1,809 patients. *Breast Cancer Research and Treatment*, 123(3), 725–
938 731. <https://doi.org/10.1007/s10549-009-0674-9>

939 Hajjari, M., & Salavaty, A. (2015). HOTAIR: an oncogenic long non-coding RNA in different cancers.
940 *Cancer Biology & Medicine*, 12(1), 1–9. <https://doi.org/10.7497/j.issn.2095-3941.2015.0006>

941 Han, Y., Feng, J., Xia, L., Dong, X., Zhang, X., Zhang, S., ... He, C. (2019). CVm6A: A Visualization
942 and Exploration Database for m(6)As in Cell Lines. *Cells*, 8(2).
943 <https://doi.org/10.3390/cells8020168>

944 Hulsen, T., de Vlieg, J., & Alkema, W. (2008). BioVenn – a web application for the comparison and
945 visualization of biological lists using area-proportional Venn diagrams. *BMC Genomics*, 9(1), 488.
946 <https://doi.org/10.1186/1471-2164-9-488>

947 Jarroux, J., Foretek, D., Bertrand, C., Gabriel, M., Szachnowski, U., Saci, Z., ... Morillon, A. (2021).
948 HOTAIR lncRNA promotes epithelial–mesenchymal transition by redistributing LSD1 at regulatory
949 chromatin regions. *EMBO Reports*, n/a(n/a), e50193.
950 <https://doi.org/https://doi.org/10.15252/embr.202050193>

951 Ko, P., Lenka, G., Chen, Y., Chuang Y., E., Tsai, M., Sher, Y., & Lai, L. (2020). Semaphorin 5A

952 suppresses the proliferation and migration of lung adenocarcinoma cells. *Int J Oncol*, 56(1), 165–
953 177. <https://doi.org/10.3892/ijo.2019.4932>

954 Konermann, S., Lotfy, P., Brideau, N. J., Oki, J., Shokhirev, M. N., & Hsu, P. D. (2018). Transcriptome
955 Engineering with RNA-Targeting Type VI-D CRISPR Effectors. *Cell*, 173(3), 665–676.e14.
956 <https://doi.org/10.1016/j.cell.2018.02.033>

957 Li, L., Liu, B., Wapinski, O. L., Tsai, M. C., Qu, K., Zhang, J., ... Chang, H. Y. (2013). Targeted
958 Disruption of Hotair Leads to Homeotic Transformation and Gene Derepression. *Cell Reports*,
959 5(1), 3–12. <https://doi.org/10.1016/j.celrep.2013.09.003>

960 Li, Y., Xia, L., Tan, K., Ye, X., Zuo, Z., Li, M., ... Xia, L. (2020). N(6)-Methyladenosine co-
961 transcriptionally directs the demethylation of histone H3K9me2. *Nature Genetics*, 52(9), 870–877.
962 <https://doi.org/10.1038/s41588-020-0677-3>

963 Liu, Jianzhao, Yue, Y., Han, D., Wang, X., Fu, Y., Zhang, L., ... He, C. (2014). A METTL3-METTL14
964 complex mediates mammalian nuclear RNA N6-adenosine methylation. *Nature Chemical Biology*,
965 10(2), 93–95. <https://doi.org/10.1038/nchembio.1432>

966 Liu, Jun, Dou, X., Chen, C., Chen, C., Liu, C., Xu, M. M., ... He, C. (2020). N6-methyladenosine of
967 chromosome-associated regulatory RNA regulates chromatin state and transcription. *Science*,
968 367(6477), 580 LP – 586. <https://doi.org/10.1126/science.aay6018>

969 Long, Y., Wang, X., Youmans, D. T., & Cech, T. R. (2017). How do lncRNAs regulate transcription?
970 *Science Advances*, 3(9), eaao2110. <https://doi.org/10.1126/sciadv.aao2110>

971 Love, M. I., Huber, W., & Anders, S. (2014). Moderated estimation of fold change and dispersion for
972 RNA-seq data with DESeq2. *Genome Biology*, 15(12), 550. <https://doi.org/10.1186/s13059-014-0550-8>

973 McDonald, O. G., Wu, H., Timp, W., Doi, A., & Feinberg, A. P. (2011). Genome-scale epigenetic
974 reprogramming during epithelial-to-mesenchymal transition. *Nature Structural & Molecular Biology*,
975 18(8), 867–874. <https://doi.org/10.1038/nsmb.2084>

976 Meredith, E. K., Balas, M. M., Sindy, K., Haislop, K., & Johnson, A. M. (2016). An RNA matchmaker
977 protein regulates the activity of the long noncoding RNA HOTAIR. *RNA (New York, N.Y.)*, 1–16.
978 <https://doi.org/10.1261/rna.055830.115>

979 Meyer, K. D., Saleto, Y., Zumbo, P., Elemento, O., Mason, C. E., & Jaffrey, S. R. (2012).
980 Comprehensive analysis of mRNA methylation reveals enrichment in 3' UTRs and near stop
981 codons. *Cell*, 149(7), 1635–1646. <https://doi.org/10.1016/j.cell.2012.05.003>

982 Mi, H., Muruganujan, A., Ebert, D., Huang, X., & Thomas, P. D. (2019). PANTHER version 14: more
983 genomes, a new PANTHER GO-slim and improvements in enrichment analysis tools. *Nucleic
984 Acids Research*, 47(D1), D419–D426. <https://doi.org/10.1093/nar/gky1038>

985 Nesterova, T. B., Wei, G., Coker, H., Pintacuda, G., Bowness, J. S., Zhang, T., ... Brockdorff, N.
986 (2019). Systematic allelic analysis defines the interplay of key pathways in X chromosome
987 inactivation. *Nature Communications*, 10(1), 3129. <https://doi.org/10.1038/s41467-019-11171-3>

988 Nguyen, E. D., Balas, M. M., Griffin, A. M., Roberts, J. T., & Johnson, A. M. (2018). Global profiling of
989 hnRNP A2/B1-RNA binding on chromatin highlights lncRNA interactions. *RNA Biology*, 15(7),
990 38

991 901–913. <https://doi.org/10.1080/15476286.2018.1474072>

992 Niu, Y., Lin, Z., Wan, A., Chen, H., Liang, H., Sun, L., ... Wan, G. (2019). RNA N6-methyladenosine
993 demethylase FTO promotes breast tumor progression through inhibiting BNIP3. *Molecular Cancer*,
994 18(1), 46. <https://doi.org/10.1186/s12943-019-1004-4>

995 Patil, D. P., Chen, C.-K., Pickering, B. F., Chow, A., Jackson, C., Guttman, M., & Jaffrey, S. R. (2016).
996 m6A RNA methylation promotes XIST-mediated transcriptional repression. *Nature*, 537(7620), 1–
997 25. <https://doi.org/10.1038/nature19342>

998 Patro, R., Duggal, G., Love, M. I., Irizarry, R. A., & Kingsford, C. (2017). Salmon provides fast and bias-
999 aware quantification of transcript expression. *Nature Methods*, 14(4), 417–419.
1000 <https://doi.org/10.1038/nmeth.4197>

1001 Pishvaian, M. J., Feltes, C. M., Thompson, P., Bussemakers, M. J., Schalken, J. A., & Byers, S. W.
1002 (1999). Cadherin-11 is expressed in invasive breast cancer cell lines. *Cancer Research*, 59(4),
1003 947–952.

1004 Portoso, M., Ragazzini, R., Brencic, Z., Moiani, A., Michaud, A., Vassilev, I., ... Margueron, R. (2017).
1005 PRC2 is dispensable for HOTAIR-mediated transcriptional repression. *The EMBO Journal*.
1006 <https://doi.org/10.15252/embj.201695335>

1007 Rafalska, I., Zhang, Z., Benderska, N., Wolff, H., Hartmann, A. M., Brack-Werner, R., & Stamm, S.
1008 (2004). The intranuclear localization and function of YT521-B is regulated by tyrosine
1009 phosphorylation. *Human Molecular Genetics*, 13(15), 1535–1549.
1010 <https://doi.org/10.1093/hmg/ddh167>

1011 Rezaul, K., Thumar, J. K., Lundgren, D. H., Eng, J. K., Claffey, K. P., Wilson, L., & Han, D. K. (2010).
1012 Differential protein expression profiles in estrogen receptor-positive and -negative breast cancer
1013 tissues using label-free quantitative proteomics. *Genes & Cancer*, 1(3), 251–271.
1014 <https://doi.org/10.1177/1947601910365896>

1015 Rinn, J. L., Kertesz, M., Wang, J. K., Squazzo, S. L., Xu, X., Brugmann, S. A., ... Chang, H. Y. (2007).
1016 Functional Demarcation of Active and Silent Chromatin Domains in Human HOX Loci by
1017 Noncoding RNAs. *Cell*, 129(7), 1311–1323. <https://doi.org/10.1016/j.cell.2007.05.022>

1018 Roberts, J. T., Porman, A. M., & Johnson, A. M. (2020). Identification of m6A residues at single-
1019 nucleotide resolution using eCLIP and an accessible custom analysis pipeline. *RNA (New York*,
1020 *N.Y.)*. <https://doi.org/10.1261/rna.078543.120>

1021 Roth, V. (2006). Doubling Time Computing. Retrieved from https://doubling-time.com/compute_more.php

1022 Roundtree, I. A., Luo, G.-Z., Zhang, Z., Wang, X., Zhou, T., Cui, Y., ... He, C. (2017). YTHDC1
1023 mediates nuclear export of N(6)-methyladenosine methylated mRNAs. *ELife*, 6.
1024 <https://doi.org/10.7554/eLife.31311>

1025 Schmitt, A. M., & Chang, H. Y. (2016). Long Noncoding RNAs in Cancer Pathways. *Cancer Cell*, 29(4),
1026 452–463. <https://doi.org/10.1016/j.ccr.2016.03.010>

1027 Shi, H., Wei, J., & He, C. (2019). Where, When, and How: Context-Dependent Functions of RNA
1028 Methylation Writers, Readers, and Erasers. *Molecular Cell*, 74(4), 640–650.

1029

1030 <https://doi.org/https://doi.org/10.1016/j.molcel.2019.04.025>

1031 Somarowthu, S., Legiewicz, M., Chillon, I., Marcia, M., Liu, F., & Pyle, A. M. (2015). HOTAIR forms an
1032 intricate and modular secondary structure. *Molecular Cell*, 58(2), 353–361.
1033 <https://doi.org/10.1016/j.molcel.2015.03.006>

1034 Takahashi, S. (2018). Molecular functions of SIRP α and its role in cancer. *Biomedical Reports*, 9(1), 3–
1035 7. <https://doi.org/10.3892/br.2018.1102>

1036 Tang, Z., Kang, B., Li, C., Chen, T., & Zhang, Z. (2019). GEPIA2: an enhanced web server for large-
1037 scale expression profiling and interactive analysis. *Nucleic Acids Research*, 47(W1), W556–W560.
1038 <https://doi.org/10.1093/nar/gkz430>

1039 The Gene Ontology resource: enriching a GOld mine. (2021). *Nucleic Acids Research*, 49(D1), D325–
1040 D334. <https://doi.org/10.1093/nar/gkaa1113>

1041 Tsai, M.-C., Manor, O., Wan, Y., Mosammaparast, N., Wang, J. K., Lan, F., ... Chang, H. Y. (2010).
1042 Long noncoding RNA as modular scaffold of histone modification complexes. *Science (New York,*
1043 *N.Y.*, 329(5992), 689–693. <https://doi.org/10.1126/science.1192002>

1044 Van Nostrand, E. L., Pratt, G. A., Shishkin, A. A., Gelboin-Burkhart, C., Fang, M. Y., Sundararaman, B.,
1045 ... Yeo, G. W. (2016). Robust transcriptome-wide discovery of RNA-binding protein binding sites
1046 with enhanced CLIP (eCLIP). *Nature Methods*, 13(6), 508–514.
1047 <https://doi.org/10.1038/nmeth.3810>

1048 Vaquero, A., Scher, M., Lee, D., Erdjument-Bromage, H., Tempst, P., & Reinberg, D. (2004). Human
1049 SirT1 interacts with histone H1 and promotes formation of facultative heterochromatin. *Molecular
1050 Cell*, 16(1), 93–105. <https://doi.org/10.1016/j.molcel.2004.08.031>

1051 Wang, Y., Zhang, H., Chen, Y., Sun, Y., Yang, F., Yu, W., ... Shang, Y. (2009). LSD1 Is a Subunit of
1052 the NuRD Complex and Targets the Metastasis Programs in Breast Cancer. *Cell*, 138(4), 660–
1053 672. <https://doi.org/https://doi.org/10.1016/j.cell.2009.05.050>

1054 Wu, L., Wu, D., Ning, J., Liu, W., & Zhang, D. (2019). Changes of N6-methyladenosine modulators
1055 promote breast cancer progression. *BMC Cancer*, 19(1), 326. [https://doi.org/10.1186/s12885-019-5538-z](https://doi.org/10.1186/s12885-019-
1056 5538-z)

1057 Wu, X., Sang, L., & Gong, Y. (2018). N6-methyladenine RNA modification and cancers. *American
1058 Journal of Cancer Research*, 8(10), 1957–1966.

1059 Wu, Yansheng, Zhang, L., Zhang, L., Wang, Y., Li, H., Ren, X., ... Hao, X. (2015). Long non-coding
1060 RNA HOTAIR promotes tumor cell invasion and metastasis by recruiting EZH2 and repressing E-
1061 cadherin in oral squamous cell carcinoma. *International Journal of Oncology*, 46(6), 2586–2594.
1062 <https://doi.org/10.3892/ijo.2015.2976>

1063 Wu, Yingmin, Yang, X., Chen, Z., Tian, L., Jiang, G., Chen, F., ... Wang, H. (2019). m(6)A-induced
1064 lncRNA RP11 triggers the dissemination of colorectal cancer cells via upregulation of Zeb1.
1065 *Molecular Cancer*, 18(1), 87. <https://doi.org/10.1186/s12943-019-1014-2>

1066 Xiao, T., Xu, Z., Zhang, H., Geng, J., Qiao, Y., Liang, Y., ... Suo, G. (2019). TP53I11 suppresses
1067 epithelial-mesenchymal transition and metastasis of breast cancer cells. *BMB Reports*, 52(6),
1068 379–384. <https://doi.org/10.5483/BMBRep.2019.52.6.173>

1069 Xu, W., Li, J., He, C., Wen, J., Ma, H., Rong, B., ... Shen, H. (2021). METTL3 regulates
1070 heterochromatin in mouse embryonic stem cells. *Nature*, 591(7849), 317–321.
1071 <https://doi.org/10.1038/s41586-021-03210-1>

1072 Yang, Z., Zhou, L., Wu, L.-M., Lai, M.-C., Xie, H.-Y., Zhang, F., & Zheng, S.-S. (2011). Overexpression
1073 of long non-coding RNA HOTAIR predicts tumor recurrence in hepatocellular carcinoma patients
1074 following liver transplantation. *Annals of Surgical Oncology*, 18(5), 1243–1250.
1075 <https://doi.org/10.1245/s10434-011-1581-y>

1076 Zaccara, S., Ries, R. J., & Jaffrey, S. R. (2019). Reading, writing and erasing mRNA methylation.
1077 *Nature Reviews Molecular Cell Biology*, 20(10), 608–624. <https://doi.org/10.1038/s41580-019-0168-5>

1079 Zhang, C., Zhi, W. I., Lu, H., Samanta, D., Chen, I., Gabrielson, E., & Semenza, G. L. (2016). Hypoxia-
1080 inducible factors regulate pluripotency factor expression by ZNF217- and ALKBH5-mediated
1081 modulation of RNA methylation in breast cancer cells. *Oncotarget*, 7(40), 64527–64542.
1082 <https://doi.org/10.18632/oncotarget.11743>

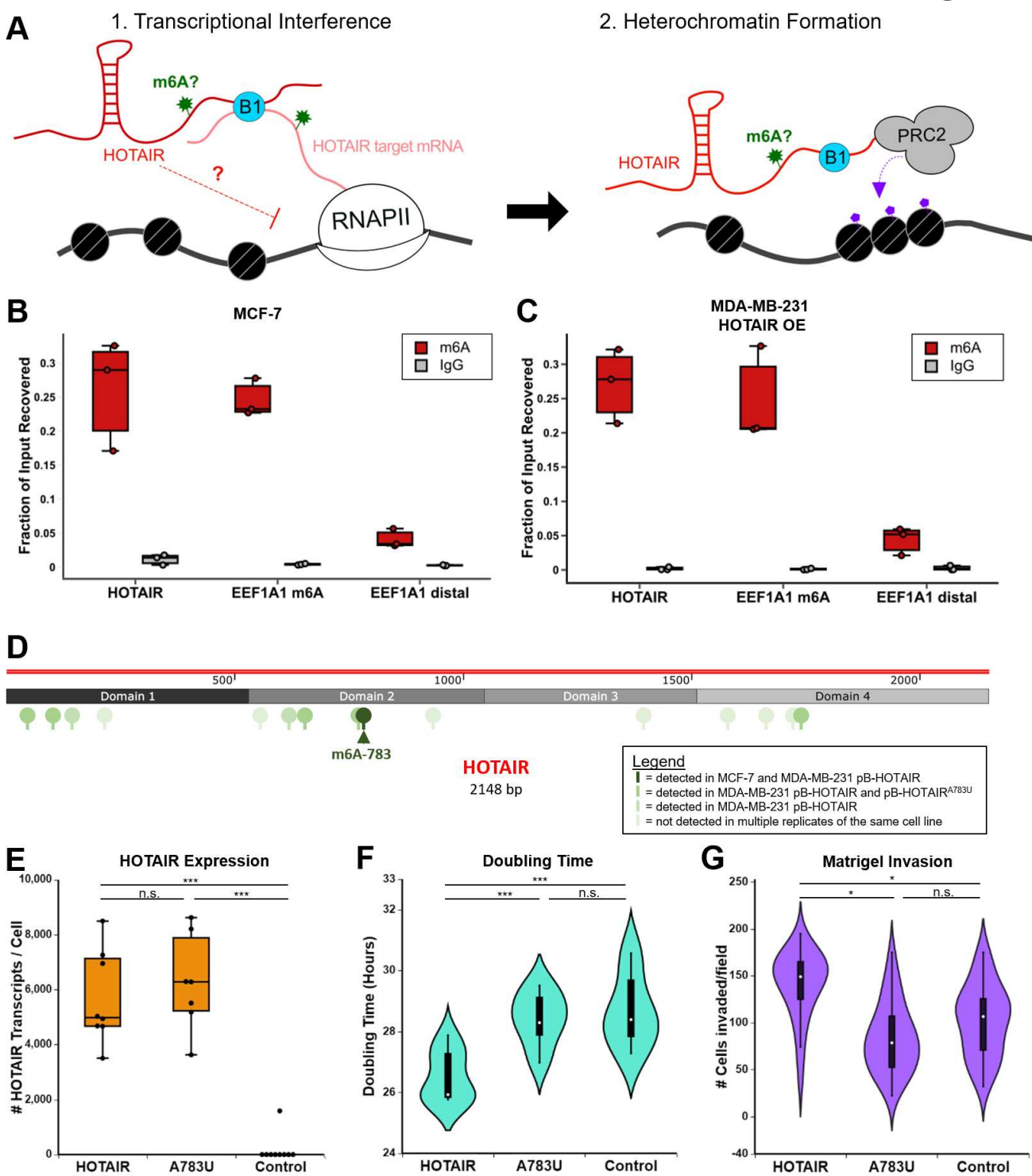
1083 Zhang, J. X., Han, L., Bao, Z. S., Wang, Y. Y., Chen, L. Y., Yan, W., ... Kang, C. S. (2013). HOTAIR, a
1084 cell cycle-associated long noncoding RNA and a strong predictor of survival, is preferentially
1085 expressed in classical and mesenchymal glioma. *Neuro-Oncology*, 15(12), 1595–1603.
1086 <https://doi.org/10.1093/neuonc/not131>

1087

1088

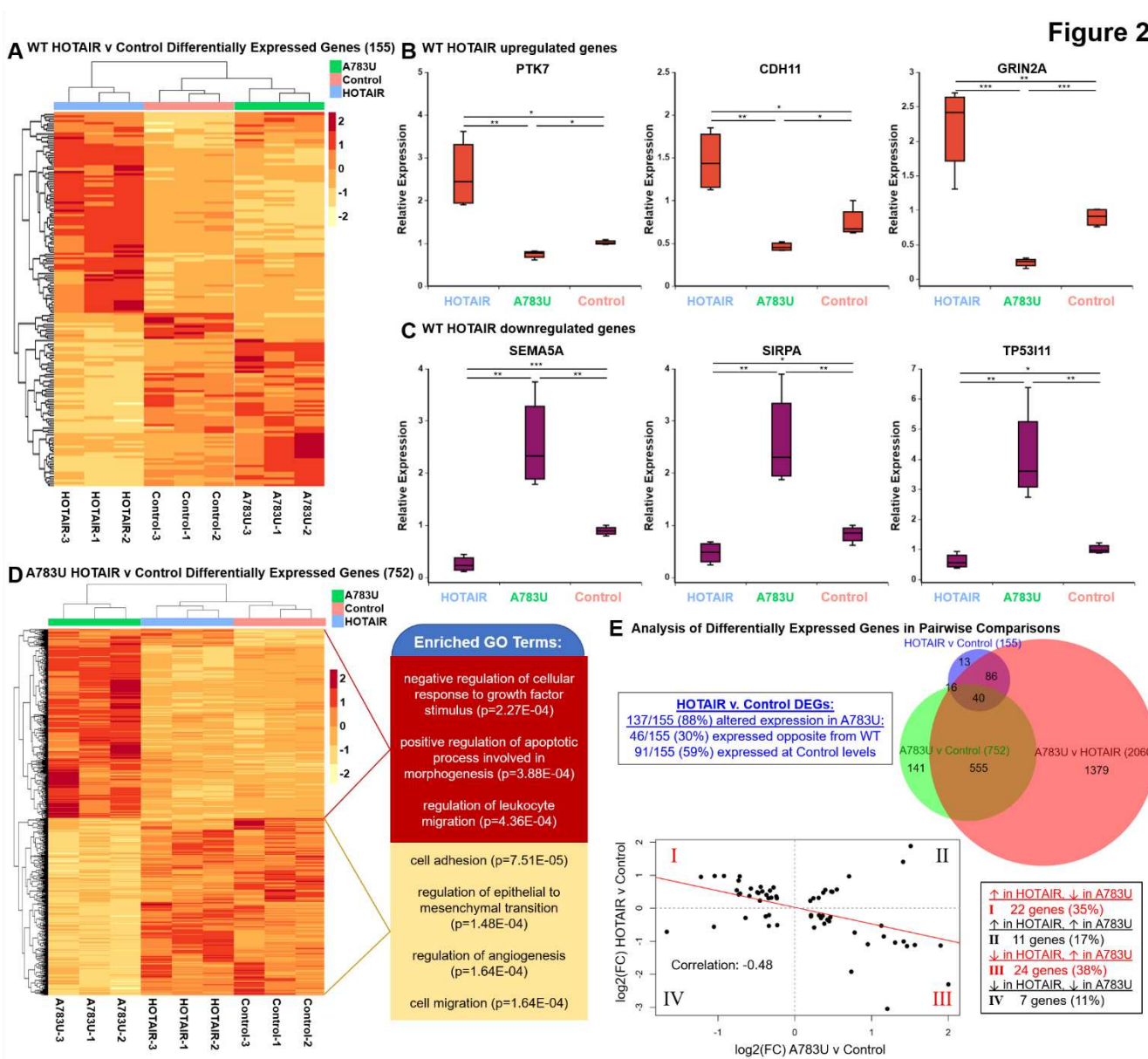
Figures and Figure Legends

Figure 1



1091 **Figure 1. LncRNA HOTAIR is m6A modified. A)** General model for HOTAIR mechanism. HOTAIR is
1092 initially recruited to its target loci via RNA-RNA interactions with its mRNA targets which is mediated by
1093 hnRNP B1. HOTAIR association with chromatin induces transcriptional interference via an unknown
1094 mechanism, promoting heterochromatin formation by PRC2 through H3K27me3. This paper investigates
1095 the role of m6A on HOTAIR. **B-C)** m6A RNA immunoprecipitation performed with an m6A antibody or
1096 IgG control in MCF-7 breast cancer cells (C) or MDA-MB-231 breast cancer cells with transgenic
1097 overexpression of HOTAIR (D). An m6A modified region in EEF1A1 (EEF1A1 m6A) is a positive control,
1098 while a distal region in EEF1A1 that is not m6A modified (EEF1A1 distal) serves as a negative control.
1099 **D)** m6A sites detected in HOTAIR-expressing cells in 6 experiments (yellow to red scale of increasing
1100 occurrences). m6A site 783 (dark red, arrow) was detected in every experiment except where it was
1101 mutated. **E)** Number of HOTAIR transcripts in MDA-MB-231 cells overexpressing WT HOTAIR, A783U
1102 HOTAIR, or an Anti-Luciferase control RNA. **F)** Doubling time of MDA-MB-231 overexpression cell lines
1103 described in (A). **G)** Quantification of cell invasion assays.

Figure 2



1104

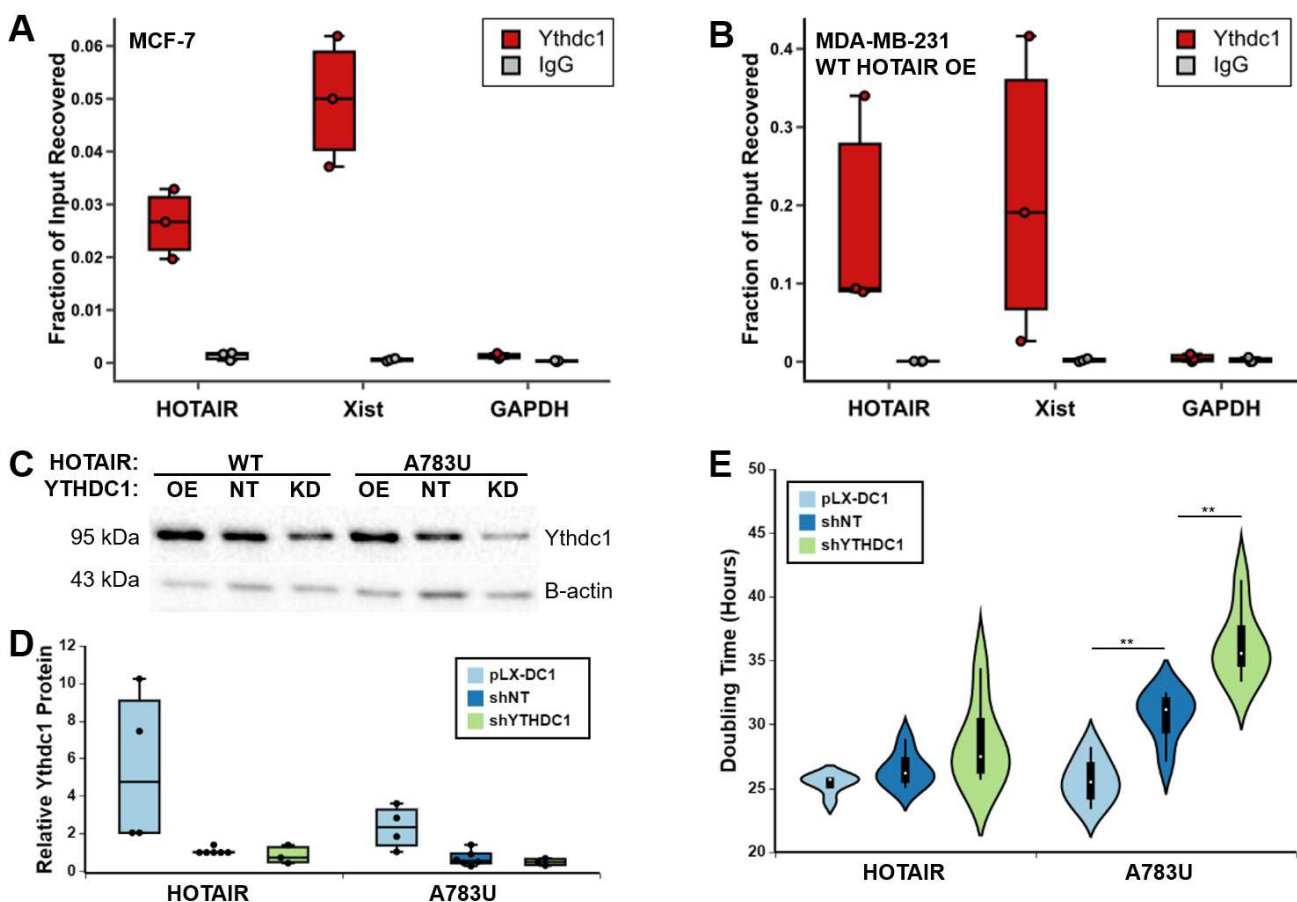
1105 **Figure 2. HOTAIR-mediated gene expression changes in breast cancer are altered by mutation of**
 1106 **A783. A)** Heatmap of Z-scores of differentially expressed genes (DEGs) between MDA-MB-231 cells
 1107 overexpressing wild-type HOTAIR versus an Anti-Luciferase control. **B-C)** qRT-PCR analysis of genes
 1108 upregulated (B) or downregulated (C) upon HOTAIR overexpression. **D)** Heatmap of Z-scores of DEGs
 1109 between MDA-MB-231 cells overexpressing A783U mutant HOTAIR versus an Anti-Luciferase control,
 1110 left. Selected significant GO terms in upregulated (red) and downregulated (yellow) genes, right. **E)**
 1111 Additional analysis of differentially expressed genes. Top, Venn diagram (created using BioVenn,
 1112 (Hulsen, de Vlieg, & Alkema, 2008)) of number of DEGs between MDA-MB-231 cells overexpressing
 1113 wild-type HOTAIR, A783U mutant HOTAIR, or an Anti-Luciferase control. Top left inset describes the

1114 direction of change in the A783U v. Control relative to the direction of the wild-type HOTAIR v. Control,
1115 based on adjusted $p < 0.1$. Bottom, correlation analysis of expression in HOTAIR v Control and A783U v
1116 Control pairwise comparisons. Linear regression was used to fit a trend line (red) over the points, with
1117 the calculated Pearson correlation coefficient included in the graph. Bottom right inset describes the
1118 number of genes in each quadrant.

1119

1120

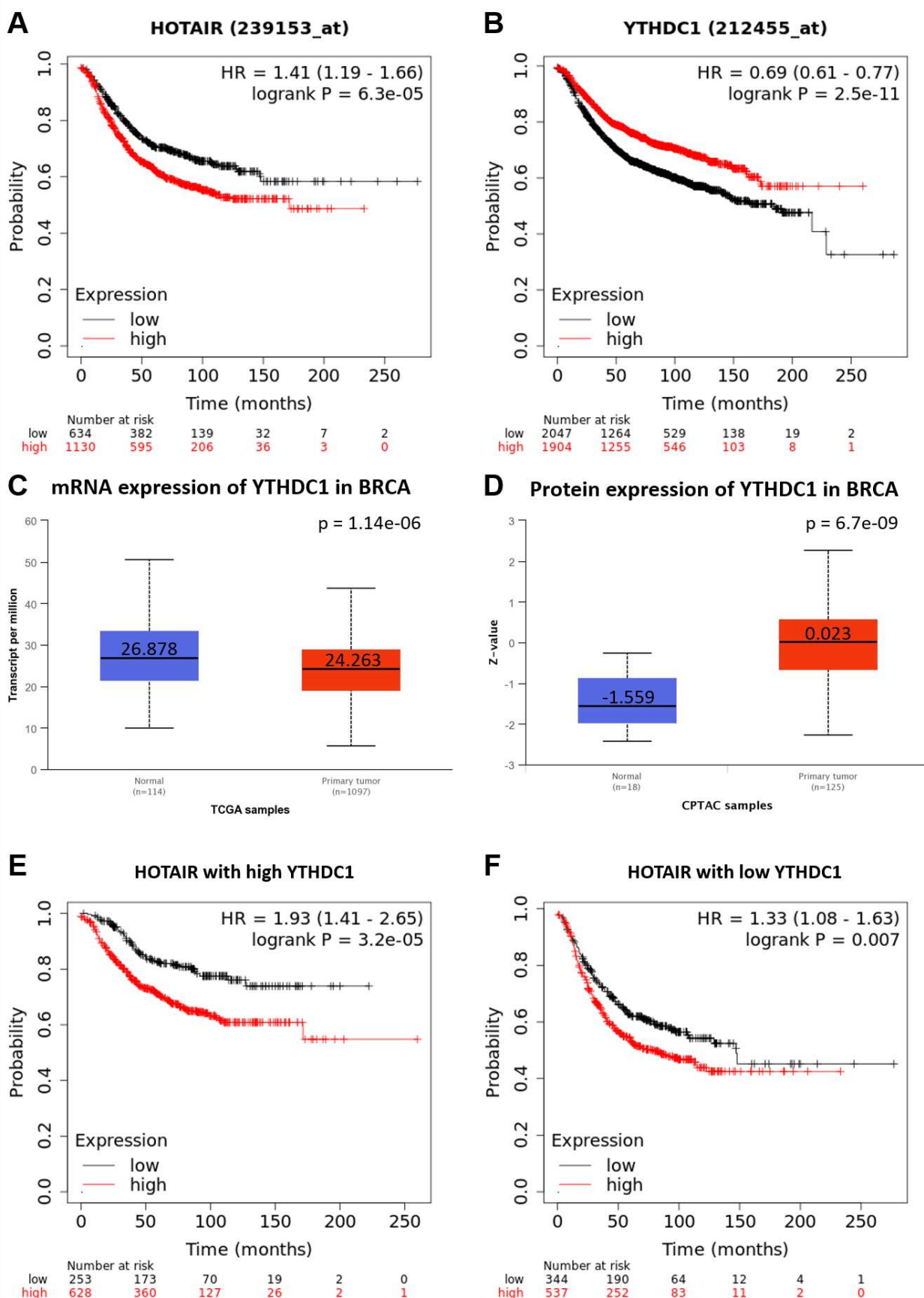
Figure 3



1121

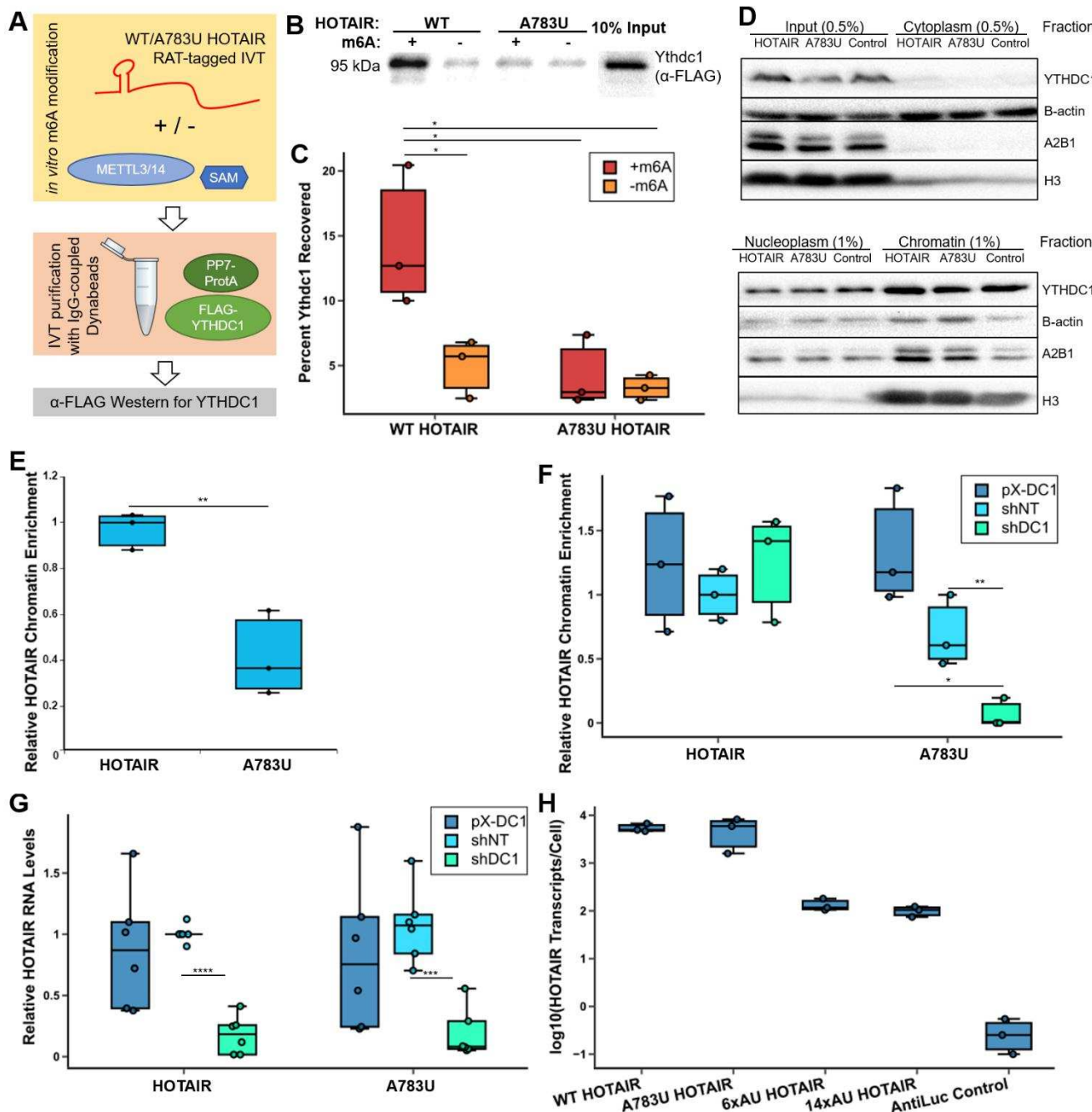
1122 **Figure 3. YTHDC1 interacts with HOTAIR and enables HOTAIR-mediated breast cancer growth. A-**
1123 **B)** YTHDC1 RIP performed in MCF-7 cells (A) or MDA-MB-231 cells overexpressing transgenic HOTAIR
1124 (B). **C)** Western blot results of YTHDC1 protein levels in pLX-DC1 overexpression, shNT control, and
1125 shDC1 knockdown MDA-MB-231 cell lines expressing WT or A783U HOTAIR. **D)** Quantification of 3
1126 replicates of (C). Protein levels of YTHDC1 were normalized to β -actin levels and are relative to the
1127 HOTAIR shNT sample. **E)** Doubling time of MDA-MB-231 cells containing WT or A783U HOTAIR and
1128 overexpression or knockdown of YTHDC1.

Figure 4



1130 **Figure 4. *YTHDC1* and *HOTAIR* in breast cancer outcomes. A-B)** Kaplan-Meier curves for recurrence-
1131 free survival of breast cancer patients with high or low expression of A) *YTHDC1* or B) *HOTAIR* generated
1132 using Kaplan-Meier Plotter(Gyorffy et al., 2010). **C-D)** Expression of *YTHDC1* C) mRNA and D) protein
1133 in normal breast tissue versus breast cancers generated with UALCAN(Chandrashekhar et al., 2017). **E-**
1134 **F)** Recurrence-free survival curves for breast cancer patients examining effect of *HOTAIR* on the
1135 background of either E) high or F) low *YTHDC1* levels, generated with Kaplan-Meier Plotter(Gyorffy et
1136 al., 2010).

Figure 5



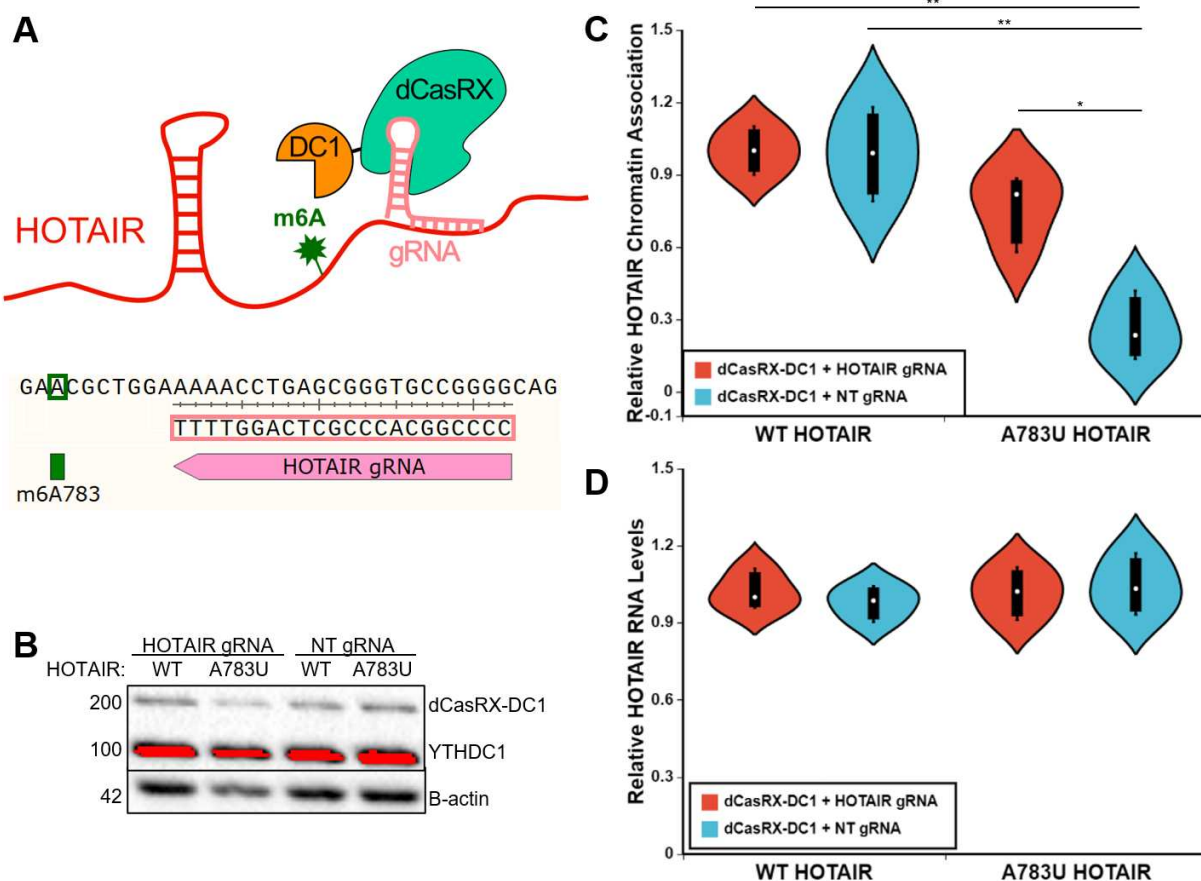
1137

1138 **Figure 5. HOTAIR m6A site 783 mediates interaction with YTHDC1 and chromatin association. A)**
 1139 Schematic of YTHDC1 pulldown experiment with m6A-modified WT and A783U HOTAIR. PP7-Protein A, cellular extract containing FLAG-tagged YTHDC1 was added, and a pulldown was performed with IgG-coupled Dynabeads. Amount of FLAG-YTHDC1 bound was assessed
 1140 domain 2 of WT or A783U HOTAIR was *in vitro* transcribed and m6A modified with purified METTL3/14.
 1141 RNA was bound to PP7-Protein A, cellular extract containing FLAG-tagged YTHDC1 was added, and a pulldown was performed with IgG-coupled Dynabeads. Amount of FLAG-YTHDC1 bound was assessed
 1142

1143 by Western blot. **B)** Anti-FLAG Western blot of pulldown experiment outlined in (A). **C)** Quantification of
1144 anti-FLAG Western blots from 3 replicates. **D)** Western blot performed on fractionation of MDA-MB-231
1145 cell lines overexpressing WT or A783U HOTAIR or Antisense-Luciferase. **E)** qRT-PCR was performed
1146 on fractionated RNA samples from MDA-MB-231 cells containing overexpression of WT or A783U
1147 HOTAIR, and chromatin association was calculated by determining the relative chromatin-associated
1148 RNA to input and normalizing to 7SL levels and relative to WT HOTAIR samples. **F)** Chromatin
1149 enrichment was calculated similarly as in (D) in MDA-MB-231 cell lines expressing WT or A783U HOTAIR
1150 with knockdown or overexpression of YTHDC1. Values are relative to HOTAIR shNT samples. **G)** qRT-
1151 PCR of *HOTAIR* RNA levels in MDA-MB-231 cell lines overexpressing WT or A783U HOTAIR containing
1152 overexpression or knockdown of YTHDC1. **H)** qRT-PCR of *HOTAIR* RNA levels in MDA-MB-231 cell
1153 lines expressing WT, A783U, 6xAU, or 14xAU HOTAIR or an AntiLuc control.

1154

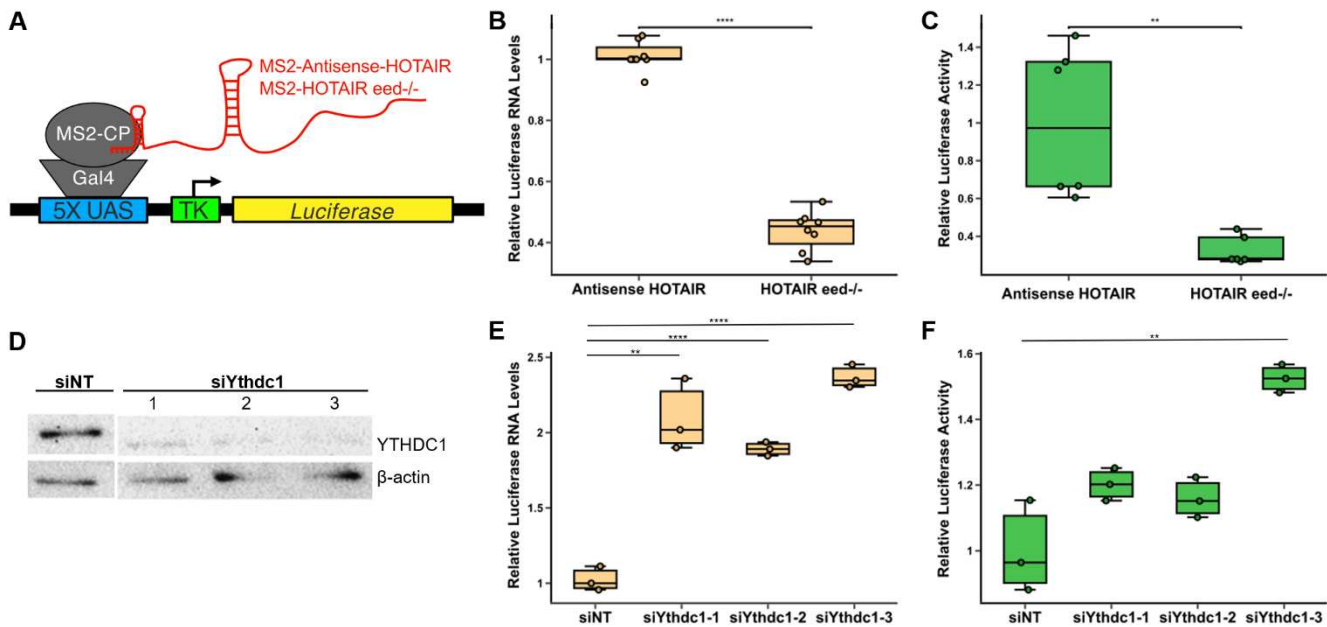
Figure 6



1155

1156 **Figure 6. Tethering YTHDC1 to A783U mutant HOTAIR restores chromatin localization**
1157 **independent of changes in RNA levels. A)** Schematic of tethering strategy using a dCasRX-YTHDC1
1158 fusion protein and a guide RNA targeted just downstream of A783 in HOTAIR. **B)** Examples of Western
1159 blots for YTHDC1 (upper) and B-actin (lower) on input, cytoplasmic, nucleoplasmic, and chromatin
1160 samples, as noted. **C)** Similar analysis described in Figure 5D-E was performed on fractionated RNA
1161 samples from cell lines overexpressing WT or A783U HOTAIR transfected with a plasmid containing
1162 dCasRX-YTHDC1 in combination with a HOTAIR or non-targeting (NT) gRNA, as noted. **D)** Relative
1163 HOTAIR RNA levels in Input samples from C.

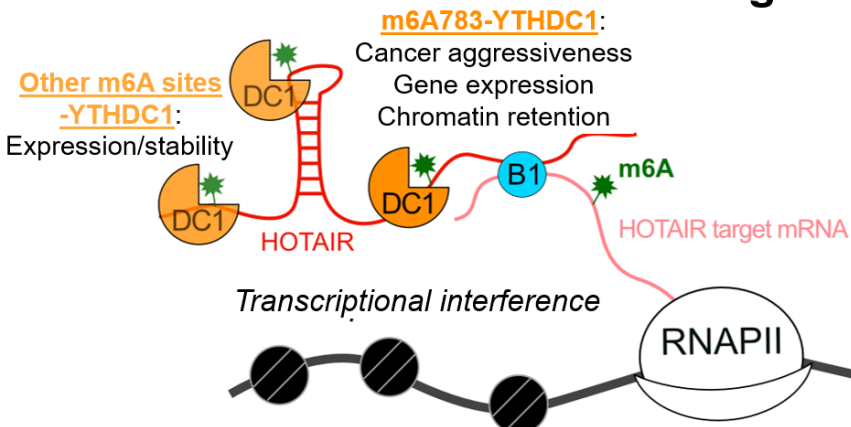
Figure 7



1164

1165 **Figure 7. YTHDC1 mediates transcriptional repression by HOTAIR.** A) Schematic of 293T cells
1166 containing MS2-Antisense-HOTAIR or MS2-HOTAIR tethered upstream of a luciferase reporter. MS2-
1167 HOTAIR tethered cells also contain a deletion of *EED*, a subunit of PRC2 that is critical for H3K27
1168 methylation. B-C) Relative luciferase RNA levels (B) and relative luciferase activity (C) in MS2-Antisense
1169 HOTAIR or MS2-HOTAIR *eed-/-* cell lines. D) Western blot of YTHDC1 in MS3-HOTAIR *eed-/-* 293T
1170 reporter cells transfected with non-targeting siRNA or 3 different siRNAs targeting YTHDC1. E-F) Relative
1171 luciferase RNA levels (E) and relative luciferase activity (F) of HOTAIR-tethered *eed-/-* cells transfected
1172 with a non-targeting siRNA or 3 different siRNAs against YTHDC1.

Figure 8



1173

1174 **Figure 8. Model of m6A and YTHDC1 effects on HOTAIR.** The main function of YTHDC1 occurs via
1175 interaction with m6A783 in HOTAIR and mediates chromatin association of HOTAIR to induce
1176 transcriptional interference of its target genes, promoting breast cancer growth. YTHDC1 also interacts
1177 with other m6A sites within HOTAIR and may mediate its high expression levels and/or stability.

1178 **Supplemental File 1. Figure supplements.**

1179 **Supplemental File 2. Supplemental tables of m6A sites identified in HOTAIR and ORFs, shRNAs,
1180 plasmids, and oligonucleotides used in this study.**

1181 **Supplemental File 3. Excel file of differentially expressed genes identified in DESeq2 pairwise
1182 comparisons.**